35. Wave, Current and Wind Loads

R. Cengiz Ertekin, George Rodenbusch

This chapter describes wave, current, and wind loads on fixed or floating offshore platforms. Both linear and nonlinear waves are discussed in deterministic and irregular seas. Linear waves are written as a subset of the more general wave theory based on the perturbation method. Nonlinear waves include Stokes waves in deep waters and cnoidal and solitary waves in shallow waters. Wave loads on both large and slender structures are formulated, and solution methods, such as the Green function method, are introduced. For large structures, linear potential theory is formulated in the frequency domain. However, time-domain methods and drift loads are also discussed. For slender structures, Morison's equation and the associated drag and inertia coefficients are introduced.

These are followed by wave–current interaction, many types of uniform and nonuniform currents, wave–current kinematics, and current-induced forces, as well as vortex-induced vibrations. A number of important quantities, such as the Doppler shift, velocity estimation through the power law, lift and drag coefficients are also introduced.

Wind forces on offshore structures are discussed through both the steady and unsteady wind profiles and forces, and through spectral analysis. Other considerations include sections on model tests and similarity laws and how various physical quantities can be scaled to prototype, both commercial and open-source computational fluid dynamics (CFD) tools, and extreme response estimation.

35.1 **Wave Loads** 787
35.1.1 Linear Waves 787
35.1.2 Nonlinear Waves 790
35.1.3 Shallow-Water Waves 791
35.1.4 Random Waves 791
35.1.5 Large Bodies 794
35.1.6 Slender-Member Bodies 798

35.2 **Current Loads** 802
35.2.1 Nonuniform Currents 802
35.2.2 Wave–Current Interaction 803
35.2.3 Wave Current Kinematics 804
35.2.4 Current-Induced Forces 804
35.2.5 Vortex-Induced Vibrations 805

35.3 **Wind Loads** 806
35.3.1 Wind-Speed Profile 807
35.3.2 Wind Spectra and Gusts 808
35.3.3 Steady-State Forces 809
35.3.4 Unsteady Forces 809

35.4 **Model Tests** 810
35.4.1 Principles and Similarity Laws 810
35.4.2 Scaling of Loads 812
35.4.3 Elastic Structures 812

35.5 **CFD Tools** 814

35.6 **Extreme Response Estimation** 814

References 816

35.1 Wave Loads

35.1.1 Linear Waves

Linear waves are characterized by the ratio of the wave amplitude to its wavelength as a *small* quantity. The fluid is assumed to be incompressible and inviscid, and the flow is irrotational, so that the particle velocity vector is given by

$$\boldsymbol{u} = \nabla\phi \,, \tag{35.1}$$

where ϕ is the velocity potential. Because of the incompressible fluid assumption, the continuity (or the con-

servation of mass) equation is given by $\nabla \boldsymbol{u} = 0$. And as a result, the continuity equation becomes Laplace's equation

$$\Delta\phi = 0\,. \tag{35.2}$$

We also have Euler's integral given by

$$\frac{\partial\phi}{\partial t} + \frac{1}{2} \parallel \nabla\phi \parallel^2 + \frac{p}{\rho} + \mathrm{g}x_2 = \frac{p_\mathrm{A}}{\rho}\,, \tag{35.3}$$

where p_A is the atmospheric pressure, ρ is the mass density of the fluid, g is the gravitational acceleration, and x_2 is the vertical coordinate (Fig. 35.1). Equation (35.3) is to be used in the determination of the pressure; it is called unsteady Bernoulli's equation by some. This equation is a result of the conservation of momentum equation which need not be simultaneously solved with the conservation of mass equation since that equation only involves a single unknown, the velocity potential.

On any material surface, whether free or not, we have the general kinematic boundary condition

$$\boldsymbol{u}\cdot\boldsymbol{n} = \frac{\partial\phi}{\partial n} = \boldsymbol{q}\cdot\boldsymbol{n}\,, \tag{35.4}$$

where $\boldsymbol{u}$ is the fluid particle velocity vector, $\boldsymbol{q}$ is the solid boundary velocity vector, and $\boldsymbol{n}$ is the unit normal vector on the boundary, pointing out of the fluid. Clearly, (35.4) is also the body-boundary condition and the seafloor boundary condition since it represents no flux through the surface. By defining the boundary surface by the equation, $F(x_1, x_2, x_3, t) = x_2 - \eta(x_1, x_3, t) = 0$, where η is the free-surface elevation, and requiring that the material derivative of F vanishes, we obtain the kinematic free-surface condition

$$\frac{\partial\phi}{\partial x_2} - \frac{\partial\eta}{\partial t} - \frac{\partial\phi}{\partial x_1}\frac{\partial\eta}{\partial x_1} - \frac{\partial\phi}{\partial x_3}\frac{\partial\eta}{\partial x_3} = 0 \quad \text{on } x_2 = \eta\,. \tag{35.5}$$

The dynamic condition on the free surface is that the pressure is continuous, that is, $p = p_\mathrm{A} \cong 0$ on $x_2 = \eta$, where we have taken the atmospheric pressure equal to zero without loss in generality. The surface tension is ignored, which means that the water waves we deal with here exclude the capillary waves (whose lengths are less than about 1.5 cm). Therefore, from Euler's integral, (35.3), we obtain the dynamic free-surface condition

$$\frac{\partial\phi}{\partial t} + \frac{1}{2}\|\nabla\phi\|^2 + \mathrm{g}\eta = 0 \quad \text{on } x_2 = \eta\,. \tag{35.6}$$

The two difficulties associated with these boundary conditions are: (i) they must be imposed on a boundary which is unknown, and (ii) they are nonlinear. Note, however, that the governing equation (35.2) is linear.

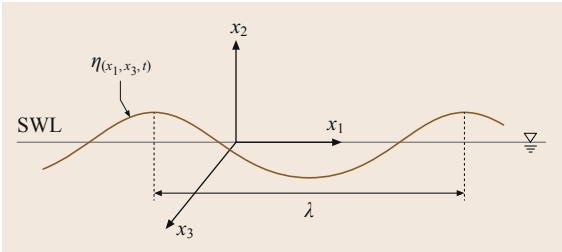

Fig. 35.1 Free surface of a wave of length λ

Perturbation Expansion

To overcome the difficulties associated with solving the nonlinear free-surface boundary conditions, one generally resorts to the use of the perturbation expansion of the quantities involved, and then linearizing the problem. To do this, one usually assumes that the wave motion is *small* and, therefore, the nonlinear terms can be discarded as a result of the argument that their magnitudes will be smaller than those of the linear terms. In this respect, one can assume that the velocity potential, as well as the surface elevation, can be expanded in a perturbation series for which a perturbation parameter ϵ is taken to be equal to, for example, Ak, where A is the wave amplitude and k is the wave number, that is, $k = 2\pi/\lambda$, where λ is the wavelength. In shallow-water wave problems, however, one would rather deal with two small parameters, one representing the nonlinearity and the other representing the dispersion of long waves.

A perturbation series is a series expansion of an unknown function about a known function, provided that the deviation of the unknown function from the known function is *small* (say the known function is the potential which can, for example, be taken as constant everywhere; this corresponds to a quiescent fluid). Then, we can write

$$\begin{aligned}
\phi &= \epsilon\phi^{(1)} + \epsilon^2\phi^{(2)} + \epsilon^3\phi^{(3)} + \cdots\,,\\
\eta &= \epsilon\eta^{(1)} + \epsilon^2\eta^{(2)} + \epsilon^3\eta^{(3)} + \cdots\,,\\
\epsilon &= Ak\,,
\end{aligned} \tag{35.7}$$

where $\phi^{(1)}$ is called the first-order potential, $\phi^{(2)}$ is the second-order potential, etc., and similarly for η, that is, $\eta^{(1)}$ is called the first-order surface elevation, $\eta^{(2)}$ is called the second-order surface elevation, etc. The expansion in (35.7) is such that when $\epsilon = 0$, there is no fluid motion; therefore, ϕ and η vanish.

Now, if the wave motion is small, meaning $\epsilon \ll 1$, we may, without giving any necessary justification, discard all the higher order terms after we substitute these

expansions in the boundary conditions. Moreover, we can expand each of the terms of the boundary conditions in a Taylor series about the still-water surface, $x_2 = 0$. For example, the time derivative of the potential is written as

$$\frac{\partial \phi}{\partial t}(x_1, x_2 = \eta, x_3, t) = \frac{\partial \phi}{\partial t}(x_1, 0, x_3, t) + \eta \frac{\partial^2 \phi(x_1, 0, x_3, t)}{\partial t \partial x_2} + \cdots . \tag{35.8}$$

Since η and ϕ are small, the higher order terms can sometimes be ignored. This means that only the linear terms involving ϕ and η have to be evaluated on the still-water level ($x_2 = 0$) instead of on the exact boundary surface, $x_2 = \eta(x_1, x_3, t)$. This is required to be consistent with the perturbation expansion. Therefore, we have the linearized versions of the boundary conditions, given by (35.5) and (35.6), as follows

$$\frac{\partial \eta^{(1)}}{\partial t}(x_1, x_3, t) = \frac{\partial \phi^{(1)}}{\partial x_2}(x_1, 0, x_3, t) \text{ (kinematic)} , \tag{35.9}$$

$$\eta^{(1)}(x_1, x_3, t) = -\frac{1}{\mathrm{g}} \frac{\partial \phi^{(1)}}{\partial t}(x_1, 0, x_3, t) \text{ (dynamic)} . \tag{35.10}$$

In summary, the first-order problem, $O(\epsilon)$ problem, becomes

$$\begin{aligned} &\Delta \phi^{(1)}(x_1, x_2, x_3, t) = 0 , \\ &\phi^{(1)}_{x_2}(x_1, -h, x_3, t) = 0 , \\ &\phi^{(1)}_{x_2}(x_1, 0, x_3, t) - \eta^{(1)}_t(x_1, x_3, t) = 0 , \\ &\phi^{(1)}_t(x_1, 0, x_3, t) + \mathrm{g}\eta^{(1)}(x_1, x_3, t) = 0 , \end{aligned} \tag{35.11}$$

where subscripts indicate differentiation with respect to the indicated variable. And for this $O(\epsilon)$ problem, the dynamic pressure is given by the linearized Euler's integral

$$p^{(1)}(x_1, x_2, x_3, t) = -\rho \phi^{(1)}_t(x_1, x_2, x_3, t), \quad x_2 < 0 , \tag{35.12}$$

anywhere in the fluid.

We can now assume that we have two-dimensional or long-crested, linear water waves so that the associated functions do not depend on the x_3-coordinate. Of course, in the case of short-crested waves, which represents the real situation in the oceans, we cannot rule out the x_3-dependence.

Let us now assume that a monochromatic wave, propagating in the positive x_1-direction, is given by

$$\eta(x_1, t) = A \cos(kx_1 - \omega t) . \tag{35.13}$$

Here, A is the wave amplitude. Equation (35.13) does not depend on time in a moving coordinate system, whose constant (phase) speed is given by $c = \frac{\omega}{k}$. In other words, the motion is steady in the moving coordinates. In a fixed coordinate system, η is a time-harmonic function. Because η is periodic, ϕ must also be periodic, so that we can write

$$\phi(x_1, x_2, t) = \mathrm{Re}\left\{ Y(x_2) \mathrm{e}^{\mathrm{i}[kx_1 - \omega t]} \right\} . \tag{35.14}$$

Equation (35.14) is a result of the separation-of-variables technique used in solving linear partial differential equations.

By enforcing the dynamic free-surface boundary condition and the no-flux sea-floor condition, the linear solution for the velocity potential can be obtained

$$\phi(x_1, x_2, t) = \frac{\mathrm{g}A}{\omega} \frac{\cosh[k(x_2 + h)]}{\cosh(kh)} \sin(kx_1 - \omega t) . \tag{35.15}$$

However, we have not yet used the kinematic free-surface condition given by the third equation in (35.11). When we enforce this condition by using (35.15), we obtain the dispersion relation

$$\omega^2 = \mathrm{g}k \tanh(kh) , \tag{35.16}$$

where h is the water depth and k is the wave number. In deep water, $kh \to \infty$, so that we have $\omega^2 = \mathrm{g}k$, and in shallow water, $kh \ll 1$, so that $\omega^2 = \mathrm{g}hk^2$.

In the deep-water case, the real part of the velocity potential of the incoming wave (or incident wave potential) becomes

$$\phi(x_1, x_2, t) = \frac{\mathrm{g}A}{\omega} \mathrm{e}^{kx_2} \sin(kx_1 - \omega t) . \tag{35.17}$$

It is useful to give particle velocity components (linear) for finite water depth by using (35.15)

$$\begin{aligned} u_1 &= \frac{\partial \phi}{\partial x_1} = \frac{\mathrm{g}Ak}{\omega} \frac{\cosh[k(x_2 + h)]}{\cosh(kh)} \cos(kx_1 - \omega t) , \\ u_2 &= \frac{\partial \phi}{\partial x_2} = \frac{\mathrm{g}Ak}{\omega} \frac{\sinh[k(x_2 + h)]}{\cosh(kh)} \sin(kx_1 - \omega t) . \end{aligned} \tag{35.18}$$

Table 35.1 Some physical quantities resulting from linear theory

Vertical particle displacement	$\zeta = A\dfrac{\sinh[k(x_2+h)]}{\sinh(kh)}\cos(kx_1-\omega t)$
Horizontal particle displacement	$\xi = A\dfrac{\cosh[k(x_2+h)]}{\sinh(kh)}\sin(kx_1-\omega t)$
Group velocity	$c_\mathrm{g} = \dfrac{1}{2}\left[1+\dfrac{2kh}{\sinh(2kh)}\right]c$
Mean energy density	$E_\mathrm{m} = \dfrac{1}{2}\rho g A^2$
Energy flux	$P = E_\mathrm{m}c_\mathrm{g}$

The total pressure (linear) can then be obtained from Euler's integral as

$$p(x_1,x_2,t) = \rho g A\frac{\cosh k(x_2+h)}{\cosh(kh)}\cos(kx_1-\omega t) - \rho g x_2\,, \tag{35.19}$$

where the first term on the right-hand side represents the dynamic and the second term represents the hydrostatic pressure.

Water particle accelerations (linear) are given by

$$\begin{aligned}\frac{Du_1}{Dt} &\cong \frac{\partial u_1}{\partial t}\\ &= \mathrm{g}Ak\frac{\cosh[k(x_2+h)]}{\cosh(kh)}\sin(kx_1-\omega t)\,, \qquad (35.20)\\ \frac{Du_2}{Dt} &\cong \frac{\partial u_2}{\partial t}\\ &= -\mathrm{g}Ak\frac{\sinh[k(x_2+h)]}{\cosh(kh)}\cos(kx_1-\omega t)\,,\end{aligned} \tag{35.21}$$

where D/Dt is the material derivative, approximated here as the local time derivative only, due to the linearity of the problem. Some other physical quantities for linear water waves are listed in Table 35.1.

35.1.2 Nonlinear Waves

To obtain the linear wave solution, the perturbation expansion introduced in the last section was truncated at $O(\epsilon)$. Clearly, this expansion can be carried out to higher orders, and this is generally done in offshore engineering and in deep-water applications, up to the fifth order. The higher order infinitesimal wave theory based on the systematic power series expansion in $\epsilon = Ak$ is due to [35.1]. The proof of convergence can be found in [35.2]. *Schwartz* [35.3] obtained the infinite-depth expansion up to $O(\epsilon^{117})$ by using a computer algorithm. However, because of the complexity of algebra and the rapid convergence of the asymptotic series, it is mostly unnecessary to consider problems of $O(\epsilon^6)$ and higher, unless, perhaps, if the water depth is very shallow. But then the Stokes expansion in shallow water gives inaccurate results in general, and thus should not be used if the water depth is shallow. Instead, a cnoidal wave theory can be used in shallow waters [35.4, 5]. The fifth-order Stokes waves, commonly used in offshore engineering, were calculated by [35.6].

After using the Taylor series expansion of the functions and its derivatives, and substituting them in the boundary conditions for each of the perturbation terms seen in (35.7), one can obtain, for example, the kinematic free-surface boundary condition at the first and second orders in two dimensions

$$\begin{aligned}&O(\epsilon): \phi^{(1)}_{x_2} - \eta^{(1)}_t = 0\,,\\ &O(\epsilon^2): \phi^{(2)}_{x_2} - \eta^{(2)}_t = \phi^{(1)}_{x_1}\eta^{(1)}_{x_1} - \phi^{(1)}_{x_2x_2}\eta^{(1)}\,.\end{aligned} \tag{35.22}$$

Note that once the first-order problem is solved, the right-hand side of the second-order boundary condition in (35.22) is known, and thus it can be treated as an applied or external pressure on the free surface located on the still-water level.

Let us consider the dynamic free-surface boundary condition given by (35.6) in two dimensions. Following the same procedure, that is, by using the Taylor series expansion of the functions in each term of the perturbation expansion, one can obtain

$$\begin{aligned}\phi_t &= \epsilon\phi^{(1)}_t + \epsilon^2(\phi^{(2)}_t + \phi^{(1)}_{x_2t}\eta^{(1)})\\ &\quad + \epsilon^3(\phi^{(3)}_t + \phi^{(1)}_{x_2t}\eta^{(2)} + \cdots) + O(\epsilon^4)\,,\\ \frac{1}{2}\{\phi^2_{x_1} + \phi^2_{x_2}\} &=\\ &\frac{1}{2}\{[\epsilon\phi^{(1)}_{x_1} + \epsilon^2(\phi^{(1)}_{x_2x_1}\eta^{(1)} + \phi^{(2)}_{x_1}) + \cdots]^2\\ &+ [\epsilon\phi^{(1)}_{x_2} + \epsilon^2(\phi^{(1)}_{x_2x_2}\eta^{(1)} + \phi^{(2)}_{x_2}) + \cdots]^2\}\\ &+ O(\epsilon^5)\,.\end{aligned} \tag{35.23}$$

Then, we have

$$\begin{aligned}&O(\epsilon): \phi^{(1)}_t + \mathrm{g}\eta^{(1)} = 0\,,\\ &O(\epsilon^2): \phi^{(2)}_t + \mathrm{g}\eta^{(2)} =\\ &\qquad -\phi^{(1)}_{x_2t}\eta^{(1)} - \frac{1}{2}(\phi^{(1)^2}_{x_1} + \phi^{(1)^2}_{x_2})\,.\end{aligned} \tag{35.24}$$

The dynamic and kinematic free-surface conditions can be combined into one equation for each $O(\epsilon)$ and $O(\epsilon^2)$

as follows

$$
\begin{aligned}
&O(\epsilon): \phi_{tt}^{(1)}(x_1,0,t) + g\phi_{x_2}^{(1)}(x_1,0,t) = 0\,,\\
&O(\epsilon^2): \phi_{tt}^{(2)}(x_1,0,t) + g\phi_{x_2}^{(2)}(x_1,0,t) =\\
&\qquad -\eta^{(1)}\left[\phi_{ttx_2}^{(1)} + g\phi_{x_2x_2}^{(1)}\right]\\
&\qquad -2(\phi_{x_1}^{(1)}\phi_{tx_1}^{(1)} + \phi_{x_2}^{(1)}\phi_{tx_2}^{(1)})\,. \qquad (35.25)
\end{aligned}
$$

The first equation in (35.25) is the combined form of the third and fourth equations, respectively, in (35.11).

It is important to note that the first-order potential, which will be given explicitly later, also satisfies the second-order problem if the water depth is infinite. In other words,

$$
\phi(x_1,x_2,t) = \frac{gA}{\omega}e^{kx_2}\sin(kx_1-\omega t) + O(\epsilon^3)\,. \qquad (35.26)
$$

However, the second-order surface elevation, that is,

$$
\eta = \epsilon\eta^{(1)} + \epsilon^2\eta^{(2)} + O(\epsilon^3) \qquad (35.27)
$$

is not the same as the first-order surface elevation given by (35.13) [35.4]. The second- and fifth-order solutions of Stokes waves are given, for example, in [35.5, Tables 4.3–4.4].

Next, we briefly discuss another type of nonlinear waves that occur when the water depth is relatively shallow.

35.1.3 Shallow-Water Waves

In relatively shallow waters, when the wavelength is greater than about eight water depths, the Stokes expansion no longer works, and an alternative wave theory must be used. One such theory is called the cnoidal wave theory as established by [35.7]. Subsequently, other cnoidal wave theories were developed by [35.4, 8–10].

The infinite length limit of cnoidal waves is known as solitary waves. These waves are generally used to model tsunami propagation and arrival times in the oceans. A number of solitary wave solution are available [35.8, 11, 12]. In more recent years, solitary waves based on the Green–Naghdi theory were also developed [35.13, 14].

Some of the equations that can be used in engineering calculations of cnoidal and solitary waves are listed in [35.5].

35.1.4 Random Waves

Irregular sea waves can be thought of as the sum of an infinite number of sinusoidal waves (each of which has a different amplitude and frequency) whose phase angles are random. In general then, the amplitude of each component wave may be represented by $A(\omega,\gamma)$, which is a random variable itself. Here, ω is the angular wave frequency and γ is the heading angle of incoming waves. Because of this randomness of waves, a probabilistic approach is necessary to describe various parameters associated with a *confused sea*. First, *Denis* and *Pierson* [35.15] introduced the probabilistic description of confused seas in marine hydrodynamics involving ship motions. As an example of the superposition of regular waves of different (however, infinitesimal) heights and frequencies, consider Fig. 35.2. Even this limited number of regular waves gives an irregular wave pattern when they are superposed. Furthermore, the resulting irregular shape is totally random, that is, a slight change in wave amplitude, frequency, or phase of the waves will result in a different pattern for irregular waves (Fig. 35.3, which also shows how the frequency domain and time domain representations of waves are related to each other in long-crested seas). Therefore, irregular waves cannot be identified by their shapes (surface elevation).

Because we cannot characterize an irregular sea by its shape, we need another criterion to base our approach on. This criterion is that the total (potential and kinetic) energy E of an irregular wave train is the sum of the energies of all components of individual waves, that is,

$$
E = \frac{\rho g}{2}\{A_1^2 + A_2^2 + \cdots\} = \frac{1}{2}\rho g\sum_{n=1}^{N}A_n^2\,. \qquad (35.28)
$$

This concept leads us to the energy spectrum in which waves of many frequencies are present. In the limit,

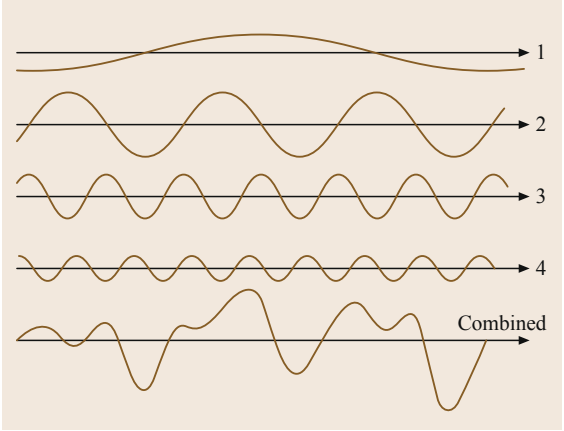

Fig. 35.2 Superposition of four regular waves with different amplitudes and lengths, shifted randomly (after [35.16])

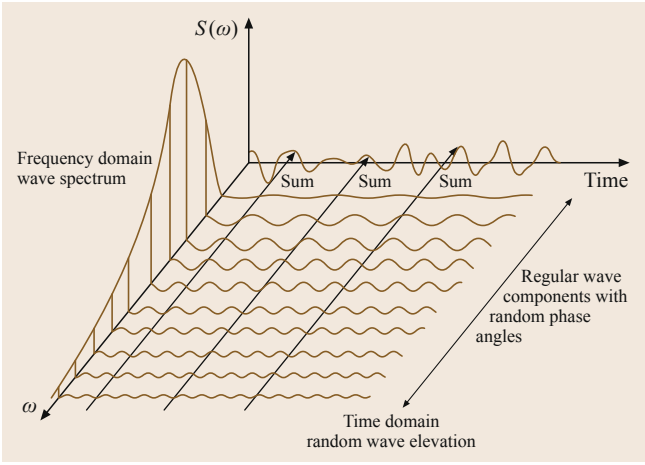

Fig. 35.3 The relation between the frequency-domain and time-domain representations of waves in long-crested seas (after [35.17])

the number of individual wave components N tends to infinity, and the summations become integrals, for example

$$\eta(x_1, x_3, t) = \mathrm{Re}\left\{\int_0^{\infty}\int_0^{2\pi} A(\omega,\gamma)\exp\{\mathrm{i}k(\omega)(x_1\cos(\gamma) + x_3\sin(\gamma)) - \mathrm{i}\omega t\}\,\mathrm{d}\gamma\,\mathrm{d}\omega\right\}, \tag{35.29}$$

where the wave amplitude $A(\omega,\gamma)$ is a random quantity. Equation (35.29) admits all possible wave directions and frequencies.

The wave spectrum can also be calculated by considering the auto-correlation function (of the surface elevation) defined by

$$R_{\mathrm{T}}(\tau) = \frac{1}{\mathrm{T}}\int_{-\frac{\mathrm{T}}{2}}^{\frac{\mathrm{T}}{2}} \eta_{\mathrm{T}}(t)\,\eta_{\mathrm{T}}(t+\tau)\,\mathrm{d}t\,. \tag{35.30}$$

The one-sided wave spectrum for a long-crested irregular wave system (unidirectional) is then given by

$$S(\omega) = \frac{1}{2\pi}\int_0^{\infty} R_{\mathrm{T}}(\tau)\cos(\omega\tau)\mathrm{d}\tau\,. \tag{35.31}$$

The total mean energy of the wave system is

$$\bar{E} = \frac{1}{2}\rho g\int_0^{\infty}\int_0^{2\pi} S(\omega,\gamma)\mathrm{d}\gamma\mathrm{d}\omega\,. \tag{35.32}$$

Since the mean square value of a monochromatic wave is $A^2/2$, we can represent a random process by

$$\eta(t) = \lim_{\Delta\omega\to 0}\left\{\sum_{n=1}^{N}\sqrt{2S(\omega_n)\Delta\omega}\cos(\omega_n t + \epsilon_n)\right\}, \quad N\to\infty\,, \tag{35.33}$$

where ϵ_n is a random phase angle uniformly distributed in the interval 0–2π, and $\omega_n = n\Delta\omega$. Even though different choices of ϵ_n would produce different time histories, the resulting wave spectrum would be the same. The mean square value of $\eta(t)$ is the area under the spectral density versus the frequency curve.

Let us consider the mean value of $\eta(t)$

$$\langle\eta(t)\rangle = \frac{1}{\mathrm{T}}\int_0^{\mathrm{T}}\eta(t)\mathrm{d}t\,, \tag{35.34}$$

and the standard deviation σ

$$\sigma = \sqrt{\frac{1}{\mathrm{T}}\int_0^{\mathrm{T}}(\eta(t) - \langle\eta(t)\rangle)^2\,\mathrm{d}t}\,. \tag{35.35}$$

The standard deviation σ is a measure of how η deviates from the mean. Water-surface elevation is assumed to have a Gaussian probability distribution, with zero mean. Thus, the variance σ^2 becomes

$$\sigma^2 = \langle\eta^2(t)\rangle = \frac{1}{\mathrm{T}}\int_0^{\mathrm{T}}\eta(t)^2\mathrm{d}t = \int_0^{\infty} S(\omega)\mathrm{d}\omega = m_0\,, \tag{35.36}$$

that is, the area under the spectral density function is the variance of $\eta(t)$ and m_0 is known as the zeroth-moment of the spectrum. In other words, the root mean square (RMS) of $\eta(t)$ is equal to the standard deviation given by (35.35) if the probability distribution is Gaussian, that is

$$\mathrm{RMS} = \sqrt{\langle\eta^2(t)\rangle} = \sqrt{m_0} = \sigma\,. \tag{35.37}$$

The spectrum of any quantity of interest, such as the motion of a platform or forces acting on it, can be obtained in a random seaway by

$$S_y(\omega) = |H(\omega)|^2 S_x(\omega) \,, \tag{35.38}$$

where the modulus (or magnitude) of $H(\omega)$ is indicated since the transfer function, $H(\omega)$, can also be a complex function of the frequency. In other words, the output spectrum is linearly proportional to the square of the transfer function. A typical transfer function could be equal to the force divided by the wave amplitude. The force clearly varies with the angular frequency ω(rad/s) (the cyclic frequency, $f = \omega/2\pi$ is used sometimes).

The transfer function, $H(\omega)$, can represent the wave force, wave run-up, surface-elevation amplitude, etc., as long as the system is linear. In other words, $L[\,]$ is an operator such that for the input $x(t)$ and the output $y(t)$, and the relation $y(t) = L[x(t)]$ between them, we must have $L[x_1(t) + x_2(t)] = L[x_1(t)] + L[x_2(t)]$. Also, for any constant α, $L[\alpha x(t)] = \alpha L[x(t)]$ needs to be satisfied. This is just the definition of a linear operator. Here, $x_1(t)$ and $x_2(t)$ are the two inputs corresponding to the two outputs $y_1(t)$ and $y_2(t)$, respectively.

For a narrow-banded spectrum (most of the energy present in waves is concentrated around a rather small interval of wave frequencies), it can be shown for any physical quantity of interest by using the Rayleigh probability distribution that

$$\bar{y}^{1/3} \cong 4.0\sqrt{m_0} = 4.0\,\sigma \,, \tag{35.39}$$

where m_0 is the area under the spectrum curve and σ is the root mean square (RMS) as given by (35.37). If, for instance, $y(t)$ is equal to the wave height, $H(t)$, we have

$$H_{1/3} = 4.0\sqrt{m_0} = 4.0\sqrt{\int_0^\infty S(\omega)\,\mathrm{d}\omega} \,, \tag{35.40}$$

where $H_{1/3}$ is called the significant wave height and $S(\omega)$ is the wave spectrum. Note that if m_0 is taken as the area under the response spectrum, $y_{1/3}$ would give the significant height (double amplitude) of the force, moment, motion, etc., whatever the response (output) corresponds to.

If one is interested in the significant amplitude response, then, for example

$$\begin{aligned} F_{1/3} &= 2.0\sqrt{m_\mathrm{R}} = 2.0\sqrt{\int_0^\infty S_\mathrm{R}(\omega)\,\mathrm{d}\omega} \\ &= 2.0\,\mathrm{RMS\ (Force)} \end{aligned} \tag{35.41}$$

will be the significant force amplitude, while $S_\mathrm{R}(\omega)$ is the force amplitude response spectrum,

$$S_\mathrm{R}(\omega) = |H(\omega)|^2\, S_W(\omega) \,, \tag{35.42}$$

where $H(\omega)$ is the force amplitude transfer function, $F(\omega)/A$, and $S_W(\omega)$ is the wave amplitude spectrum.

Once the significant response is known, it is possible to predict (if the Rayleigh distribution is valid) the short-term design extreme by the following formula (for a derivation of this equation, see for example [35.18, p. 319]),

$$y_\mathrm{extreme} = y_{1/3}\left(\frac{1}{2}\log\frac{N}{0.01}\right)^{1/2} \,, \tag{35.43}$$

where N is the number of waves expected to be encountered during a storm. For example, if the storm lasts for 3 hours and the average wave period is 15 s, then $N = 3 \times 60 \times 60/15 = 720$, and, therefore, $y_\mathrm{extreme} = 1.5584\, y_{1/3}$.

Sometimes we may know the spectrum given as a function of one quantity, say cyclic wave frequency or period or encounter frequency, and we may need to convert it to a wave spectrum as a function of another quantity. To do this, one has to keep in mind that the energy content of the waves must remain the same no matter what coordinate system is used (this is called *Galilean Invariance*), including the steadily moving one. It is common, for example, to see that the cyclic wave frequency, $f = 1/T$ (Hz), is used in calculations. In such cases, one can convert the angular-frequency spectrum into the cyclic-frequency spectrum by writing

$$S(f)\mathrm{d}f = S(\omega)\mathrm{d}\omega,\ \omega = 2\pi f \ \Rightarrow\ S(f) = 2\pi S(\omega) \,. \tag{35.44}$$

So far, we have concentrated on the long-crested wave spectrum. The waves in the ocean are, in fact, short crested, meaning that they move in different directions in general. If waves are multidirectional, and, therefore, are short crested, with a dominant wave heading angle γ, the directional wave-energy spectral density can be written as

$$\begin{aligned} &\bar{S}_\mathrm{W}(\omega,\theta) = S_\mathrm{W}(\omega)G(\theta) \,, \\ &G(\theta) = \frac{2}{\pi}\cos^2\theta \,, \\ &-\frac{\pi}{2} \le \theta \le \frac{\pi}{2} \,, \end{aligned} \tag{35.45}$$

where θ, the heading angle of each component wave, is measured from the axis of the dominant wave heading,

and $G(\theta)$ is called the spreading function, which, by assumption, is set to zero if $|\theta| > \pi/2$. Note that there exist spreading functions that are different from (35.45). This is because of a better fit of a particular spreading function to observational data at a specific ocean site.

The wave spectrum for a given location is, in general, not available from observational data. As a result, we must use one or more of a number of formulas developed for estimating the wave spectrum. Here, we summarize some of them, and the reader is referred to other works for more detailed analysis of and references on the subject [35.5] or [35.19].

The Bretschneider spectrum is based on the significant wave height H_s and peak wave (angular) frequency, $\omega_p = 2\pi/T_p$, where T_p is the peak period of the wave spectrum, that is, it is a two-parameter spectrum. For fully developed seas, the wave spectrum is

$$S(\omega) = \frac{5H_s^2}{16\omega_p}\frac{1}{(\omega/\omega_p)^5}\exp\left\{-\frac{5}{4}\left(\frac{\omega}{\omega_p}\right)^{-4}\right\} . \tag{35.46}$$

The dimension of the wave spectrum is L^2T. An example of a Bretschneider spectrum is shown in Fig. 35.4.

The Pierson–Moskowitz (P–M) spectrum is based on the wind speed U_w(m/s) alone, it is a one-parameter spectrum, and is given by

$$S(\omega) = \frac{\alpha g^2}{\omega^5}\exp\left(-\frac{B}{\omega^4}\right) , \tag{35.47}$$

where $\alpha = 8.1\times10^{-3}$ is Phillips' constant, $B = 0.74(g/U_w)^4$, and g is the gravitational acceleration. It is possible to express the P–M spectrum in terms of the significant wave height, H_s, that is the average height of the highest one-third of the waves. Recall that H_s is given by (35.40)

$$H_s = 4.0\sqrt{m_0} = 4.0\sqrt{\int_0^\infty S(\omega)\mathrm{d}\omega}$$
$$= \frac{2{U_w}^2}{g}\sqrt{\frac{\alpha}{0.74}} \quad \text{or} \quad {U_w}^{-4} = \frac{0.044}{g^2(H_s)^2} , \tag{35.48}$$

where we used (35.47). Therefore, we can now write the one-parameter P–M spectrum in terms of H_s

$$S(\omega) = \frac{8.1-3g^2}{\omega^5}\exp\left(-0.032\frac{g^2}{\omega^4(H_s)^2}\right) . \tag{35.49}$$

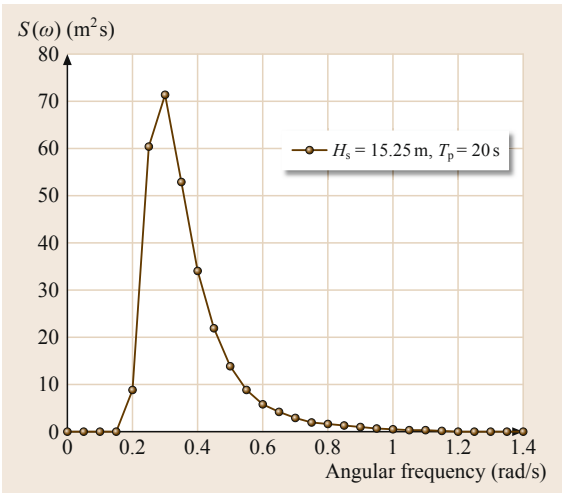

Fig. 35.4 Bretschneider spectrum for significant wave height of 15.25 m and peak period of 20 s

35.1.5 Large Bodies

When an offshore structure is *large* (generally the dimensions of the structure and perhaps even of each member is not small compared with the wavelength), one would assume that the viscous effects are much smaller than the inertial effects as far as the wave loads are concerned. In this section, we discuss wave loads on large structures by using linear potential theory valid for rather small wave slopes and under the assumptions of inviscid and incompressible fluid and irrotational flow.

Potential Theory

Since we have a linear system, meaning that the governing equation (Laplace's equation) and the boundary conditions do not contain any nonlinear terms, all physical quantities related to the response should be linearly proportional to wave amplitude. As a result, the complicated problem of a freely floating structure impacted by linear waves can be decomposed into multiple problems, each of which are easier to solve. The sum of all the solutions will then be the solution of the complicated problem, as long as the linearity assumption made holds true, that is, that the wave slope is small.

Consider a freely floating body in the *absence* of forward motion. We assume that the body makes *small* motions in six degrees of freedom, and that they can be written as

$$x_j = x_j^0 e^{-i\omega t} , \quad i = \sqrt{-1}, \quad j = 1, 2, \ldots, 6 . \tag{35.50}$$

Each x_j, $j = 1, 2, 3$, refers to the translational displacements of surge, heave, and sway, respectively, and each x_j, $j = 4, 5, 6$, refers to the angular displacements (or rotations) of roll, yaw, and pitch, respectively, and x_j^0 denotes the complex amplitude of the motion.

The complex total potential due to the interaction of waves with the body can be written in a compact form as

$$\Phi_{\mathrm{T}} = \sum_{j=0}^{7} \phi_j(x_1, x_2, x_3) \mathrm{e}^{-\mathrm{i}\omega t} \,, \tag{35.51}$$

where $\phi_0 \equiv \phi_I$ is the incoming wave potential, ϕ_j, $j = 1, 2, \ldots, 6$, are the radiation potentials, and $\phi_7 \equiv \phi_D$ is the diffraction potential, all being complex functions of the independent spatial variables. The incoming wave potential is only due to the periodic linear waves propagating in the absence of the body, the diffraction potential is due to a fixed body impacted by the incoming waves, and the radiation potentials are due to a body oscillating in a prescribed mode of motion, one at a time, and in the absence of any incoming waves.

Each potential in (35.51) must satisfy

$$\begin{aligned} \nabla^2 \phi_j(x_k) &= 0, \quad x_k \in D \,, \\ \frac{\partial \phi_j(x_k)}{\partial x_2} - \frac{\omega^2}{\mathrm{g}} \phi_j(x_k) &= 0, \quad x_k \in S_{\mathrm{f}} \,, \\ \frac{\partial \phi_j(x_k)}{\partial x_2} &= 0, \quad x_k \in S_{\mathrm{s}} \,, \end{aligned} \tag{35.52}$$

for $j = 0, 1, 2, \ldots, 7$ and $x_k \equiv (x_1, x_2, x_3)$ (Fig. 35.5). The sea-floor condition (as used here) implies that the water depth is constant (although this is not a necessary assumption in general).

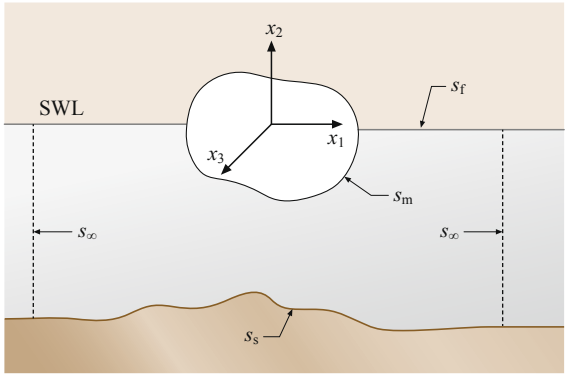

Fig. 35.5 A control volume in the fluid, bounded by the body, still-water surface, sea floor, and a large control cylinder of radius R

In addition, we must have the following body-boundary conditions to be satisfied

$$\begin{aligned} \frac{\partial \phi_j(x_k)}{\partial n} &= n_j \,, \; j = 1, 2, \ldots, 6, \; x_k \in S_{\mathrm{m}}; \\ \frac{\partial \phi_7(x_k)}{\partial n} &= -\frac{\partial \phi_0(x_k)}{\partial n} \,, \; x_k \in S_{\mathrm{m}} \,. \end{aligned} \tag{35.53}$$

And all ϕ_j, $j = 1, 2, 3, \ldots, 7$, except the incident wave-potential, must also satisfy the Sommerfeld radiation condition:

$$\lim_{r \to \infty} \left[\sqrt{r} \left(\frac{\partial}{\partial r} - ik \right) \phi_D \right] = 0 \,. \tag{35.54}$$

This equation basically states that the particle velocities $\to 0$ as $r \to \infty$ and that the waves are outgoing. Equation (35.54) is called the radiation condition (or the Sommerfeld condition) for a three-dimensional (3-D) body of bounded extent in a fluid (with a free surface) of unbounded extent on the horizontal plane. Note that

$$r = \sqrt{x_1^2 + x_3^2}$$

on the horizontal plane. This equation must be satisfied by the diffraction and radiation potentials, but not by the incoming potential.

The total pressure can be obtained from linearized Euler's integral

$$p_{\mathrm{T}} = -\rho \mathrm{g} x_2 - \rho \frac{\partial \Phi_{\mathrm{T}}}{\partial t} \,; \tag{35.55}$$

and the total force ($j = 1, 2, 3$) and moment ($j = 4, 5, 6$) are obtained from

$$F_{\mathrm{T}j} = -\int_{S_{\mathrm{m}}} p_{\mathrm{T}} n_j \, \mathrm{d}S \,, \quad j = 1, 2, \ldots, 6 \,. \tag{35.56}$$

The hydrostatic forces and moments due to the first term on the right hand side of (35.55) can be written as

$$F_{\mathrm{S}i} = -k_{ij}^{(\mathrm{S})} x_j \,, \quad i, j = 1, 2, \ldots, 6 \,, \tag{35.57}$$

where $k_{ij}^{(\mathrm{S})}$ are the hydrostatic stiffness (or restoring) coefficients, $k_{22}^{(\mathrm{s})} = \rho \mathrm{g} A_{\mathrm{WP}}$ is the restoring coefficient in heave, where A_{WP} denotes the water-plane area of the body. Because there is no restoration in the horizontal plane, it is clear that $k_{ij}^{(\mathrm{s})} = 0$ if $i, j = 1, 3, 5$. Also, note that, in a linear system and for a rigid body, $k_{ij}^{(\mathrm{S})} = k_{ji}^{(\mathrm{S})}$, that is, the hydrostatic stiffness matrix (or tensor) is

symmetric. For elastic (or deformable) bodies, this can also be shown [35.20].

The total forces and moments given by (35.56) includes the hydrostatic, wave-exciting and radiation forces, and moments. The wave-exciting forces can be written as

$$F_{Wj} = -\rho e^{-i\omega t} \int_{S_m} \left(\frac{\partial \phi_0}{\partial t} + \frac{\partial \phi_7}{\partial t} \right) n_j dS$$
$$= AE_j e^{-i\omega t}, \quad j = 1, 2, \ldots, 6, \tag{35.58}$$

where E_j is the complex amplitude of the exciting force divided by the wave amplitude A. Note that (35.58) includes both the Froude–Krylov force ($\partial\phi_0/\partial t$ term) and the scattering force ($\partial\phi_7/\partial t$ term).

The hydrodynamic (or radiation) forces due to the motion of the body in each mode can be determined, once the radiation potentials are solved for. They are given by

$$F_{Ri} = -\mu_{ij}\ddot{x}_j - \lambda_{ij}\dot{x}_j, \quad i, j = 1, 2, \ldots, 6, \tag{35.59}$$

where

$$\mu_{ij} = \rho \int_{S_m} \phi_j^{(R)} \frac{\partial \phi_i^{(R)}}{\partial n} \, dS,$$
$$\lambda_{ij} = \rho\omega \int_{S_m} \phi_j^{(I)} \frac{\partial \phi_i^{(R)}}{\partial n} \, dS, \tag{35.60}$$

where $\phi_j^{(R)}$ is the real and $\phi_j^{(I)}$ is the imaginary part of j-th radiation potential. The components of the second-order tensor μ_{ij} are called the added-mass coefficients, and λ_{ij} are called the wave-damping or, simply, damping coefficients. Note that, in the unbounded-fluid case, there is no free surface and, as a result, there is no wave generation. And, therefore, the damping coefficients do not exist since no energy is carried by waves toward infinity. See, for example, [35.21] for some added-mass and damping coefficients for a floating structure of a semisubmersible type.

By considering a control volume enclosed by the free surface, the body surface, sea floor, and an imaginary cylinder at $r = \infty$, one can show that $\mu_{ij} = \mu_{ji}$ and $\lambda_{ij} = \lambda_{ji}$ by using Green's second identity. Note that these results are valid if there is no forward motion. It can also be shown that the average rate at which work is done by the body upon the fluid is directly proportional to λ_{ij}, and, therefore, that the matrix λ_{ij} must be positive definite for all ω. In particular, $\lambda_{ii} > 0$ for all $i = 1, 2, \ldots, 6$ and ω, but in some cases $\lambda_{ij}, i \neq j$ may be negative [35.22].

There may be mooring lines which are attached to the body to keep it in location. These mooring lines tend to restore the motion of the body, and, thus, can be treated as restoring coefficients

$$F_{Mi} = -k_{ij}^{(M)} x_j, \quad i, j = 1, 2, \ldots, 6. \tag{35.61}$$

And they can provide restoring (however small) in all modes of motion unlike the hydrostatic restoring.

We can now assemble the forces and moments to obtain

$$F_{Ti} = -(k_{ij}^{(S)} + k_{ij}^{(M)})x_j - \mu_{ij}\ddot{x}_j - \lambda_{ij}\dot{x}_j + AE_i e^{-i\omega t}, \tag{35.62}$$

where we have also included the mooring line loads in (35.62) (they were not included in (35.56)).

We are now ready to consider Newton's equations which govern the motions of a body. These equations can be written as

$$F_{Ti} = m_{ij}\ddot{x}_j, \quad i, j = 1, 2, \ldots, 6, \tag{35.63}$$

where

$$m_{11} = m_{22} = m_{33} = m, \; m_{44} = I_1, \; m_{55} = I_2,$$
$$m_{66} = I_3, \; m_{54} = m_{45} = -I_{12}, \; m_{46} = m_{64} = -I_{13},$$
$$m_{56} = m_{65} = -I_{23},$$
$$I_{jk} = \int_V \bar{x}_j \bar{x}_k \rho_B \, dV, \; I_1 = I_{22} + I_{33}, \; I_2 = I_{11} + I_{33},$$
$$I_3 = I_{11} + I_{22}, \tag{35.64}$$

where any unspecified mass or mass moment, m_{ij}, is zero, provided that F_{Tj} refers to a coordinate system which is fixed in the mean position, S_m, of the body, and whose origin coincides with the center of gravity of the body. Here, ρ_B is the mass density of the body and I_{ij} are called the moment of inertia coefficients when $i = j$, and products of inertia when $i \neq j$ [35.23].

We can now set (35.62) equal to (35.63) and arrange the equation by moving some terms around to obtain

$$(m_{ij} + \mu_{ij})\ddot{x}_j + \lambda_{ij}\dot{x}_j + (k_{ij}^{(S)} + k_{ij}^{(M)})x_j = AE_i e^{-i\omega t}. \tag{35.65}$$

Considering (35.50), we can write the equations of motion given by (35.65) as

$$\frac{x_j^0}{A} = \left[-\omega^2(m_{ij} + \mu_{ij}) - i\omega\lambda_{ij} + \left(k_{ij}^{(S)} + k_{ij}^{(M)}\right) \right]^{-1} E_i. \tag{35.66}$$

Recalling that x_j^0 is complex, we can write it as

$$x_j^0 = x_j^{0R} + \mathrm{i}x_j^{0I} = |x_j|\mathrm{e}^{-\mathrm{i}\delta} ,$$

where δ is the phase angle of the motion relative to the incoming-wave crest. As a result, (35.66) becomes two sets of simultaneous 6×6 linear equations to be solved for the motion response, $|x_j^0|/A$. These motion responses are commonly called transfer functions. The square of a transfer function is sometimes known as the response amplitude operator (RAO). However, it is not uncommon that a transfer function, itself, is called an RAO, rather than its square. RAOs are used in irregular sea analysis to determine the random or stochastic response of a floating body in random waves. It is also noted that the term *transfer function* is also used for wave forces or moments per unit wave amplitude A.

Solution Methods

The boundary-value problems above can be solved to obtain the diffraction and radiation potentials so that the hydrodynamic coefficients and wave loads can be calculated. These potentials can be evaluated using the 3-D source-distribution method [35.24–26]. The pulsating source potential, which is a complex function, in infinite water depth can be found in [35.27, Art. 13]. This Green function can be written in an alternate form [35.28]. A different series expansion of the Green function is also given in [35.27]. Although this series expansion is more accurate and more computationally efficient to evaluate, compared with the integral form given in [35.27], it is limited to cases where kr is not very small. On the other hand, the evaluation of the Green function given by [35.28] is much more efficient, and no difficulty with regard to the size of kr is expected.

The solution of the integral equation for the unknown strengths of the distributed sources requires the discretization of the body surface by panel elements. Once the unknown strengths of the sources are determined on the body boundary (discretized by constant panels) by enforcing the body boundary condition, the diffraction and radiation potentials can be determined. These calculations can be performed by a number of commercially available computer programs.

A Green function is also called a source function, and it is one of the bases for finding solutions to diffraction and radiation problems in coastal and offshore engineering. A numerical method, called the boundary-element method (BEM), uses this approach. However, the BEM uses the simple Rankine source rather than the complicated Green function, and, as a result, all boundaries of the flow field need to be discretized. The Green function (GFM), requires the discretization of the boundaries on which there are distributed singularities with unknown strengths. For example, in the case of the linear problem of a floating body, only the body boundary need to be discretized. The BEM or the GFM is in contrast with the finite-element method (FEM) which requires that the entire fluid domain and its boundaries be discretized to solve for the velocity potential, and, therefore, the velocities. For more information on the BEM, the readers are referred to [35.29].

One of the alternative methods for solving hydrodynamic problems is the FEM. The disadvantage of this method compared to the GFM, provided that a particular Green function exists and is available, is that ϕ has to be calculated everywhere inside the domain. On the other hand, i) the FEM results in a banded matrix which can be solved efficiently, ii) the function calculated in the FEM is simpler, and iii) the FEM requires less knowledge of mathematics and fluid mechanics than the GFM does. Another numerical method that can be used is the finite-difference method, although it is used infrequently in fluid–structure interaction problems involving floating bodies.

Time-Domain Methods

Sometimes, the frequency-domain method discussed before is inadequate to incorporate certain nonlinearities and/or interactions in the system, and, as a result, one needs to resort to a time-domain method of calculating the loads and/or motions of an offshore structure. Typical examples could include problems involving the current and wave interaction, and low-frequency motions of platforms. These time-domain methods are based, in most cases, on the hydrodynamic coefficients and loads that have been previously calculated through a frequency-domain method and utilize the fact that the frequency and time contents of a system are related through the Fourier transforms. It is noted that some of the loads and/or the equations of motion could be nonlinear in these calculations.

Memory effects are included through the velocity-based convolution integrals. The memory effects considered are largely based on the early works of [35.30, 31] and [35.22] in the application of linear potential theory in the time domain, and on the work of [35.32]. Viscous effects may be included through the nonlinear drag term of Morison's equation. An earlier review of linear and nonlinear methods of time-domain calculations of motions can be found in [35.33]. This is an important reference as it is not always possible to use a time-domain method based on the linear hydrodynamic coefficients or exciting forces obtained through a frequency-domain method, by a Green function panel method, as some physical events are nonlinear and even transient.

There are many applications of the mentioned time-domain methods applied to various ocean engineering

problems, including to wave-energy conversion (WEC) problems [35.34]. There also are software packages, for example, ANSYS AQWA, that use some of these methods.

Drift Loads

The first-order wave loads discussed so far are time harmonic and, therefore, do not produce a steady component. This is mainly because the second-order component of the pressure on the body was assumed to be zero in the linear problem, see (35.3). Clearly, if this term was included, the time-mean force would have been of second order even though the first-order (linear) potential was used. Moreover, if a body is surface-piercing, there would be an additional term related to the runup on the body. In regular waves, this mean force is called the drift force in brief. In irregular waves, there is the mean drift force, but in addition there is also the slowly varying drift force. All these forces, although smaller in magnitude compared with the first-order forces, may become very important especially for bodies that are moored, as they may amplify motions due to a possible resonance in the system.

Maruo [35.35] showed that the mean drift force can be shown to be proportional to the square of the reflected wave amplitude, and since the reflected wave can be thought of as the reflection coefficient times the incoming wave amplitude, the mean drift force can be seen to be proportional to the square of the incoming wave amplitude. Reference [35.36] used the far-field radiation potentials (momentum) approach to obtain the drift forces on a floating body, and these were used later by [35.25] to calculate the drift force and moment on a floating body. The momentum approach results in expressions that involve the Kochin function. *Pinkster* [35.37], on the other hand, used the near-field potentials to calculate the mean drift forces and moments in all six degrees of freedom, and this approach was used later by [35.38] in conjunction with the panel method based on the Green-function method for a 3-D floating structure. These studies are for single bodies; multi-body calculations of drift forces became important later due to plans to build very large floating stuctures (VLFS) [35.39, 40].

The slowly varying component of the drift force on rigid bodies in irregular waves appears to have been first studied experimentally by [35.41] and later theoretically by [35.42].

35.1.6 Slender-Member Bodies

A slender member of a body is defined as a structural member whose characteristic dimension, for example, diameter, is *small* compared to the wavelength. With this in mind, we discuss Morison's equation which is sometimes used in offshore engineering during the preliminary design stage.

Morison's Equation

Wave forces on cylindrical structural members, such as the pontoons or columns of a platform or a pile that extends to the sea floor, when both the inertia and viscous forces are important, are discussed here. Due to the nonlinear nature of the Navier–Stokes equations and the boundary conditions, many have attempted to simplify the computation of wave forces on cylindrical piles. Most of the studies have been based on the experimental determination of the inertia and drag coefficients that appear in Morison's equation [35.43]. Morison's equation was developed as an ad hoc approach to a limited set of experimental data. However, because of the importance of cylindrical piles both in offshore engineering (jack-up platforms) and coastal engineering (pier piles, bridge columns, etc.), there have been many investigations on the proper coefficients to be used in almost every different case that one can imagine. A few of the different cases include inclined cylinders, group of cylinders, roughened cylinders, and horizontal cylinders [35.5].

The original form of Morison's equation is given by

$$\delta F = (1 + C_a)\rho\pi \left(\frac{D}{2}\right)^2 \dot{u}_1 + \frac{1}{2}\rho D C_d u_1 |u_1| \,, \tag{35.67}$$

where δF is the sectional (in the x_2 (vertical) direction) horizontal force, D is the diameter of the vertical pile, u_1 is the wave horizontal velocity, $\dot{u}_1$ is the wave horizontal acceleration, C_a is called the added-mass or virtual-mass coefficient, and C_d is the form-drag coefficient. C_a and C_d are dimensionless. $C_m = (1 + C_a)$ is called the inertia coefficient. Note that u_1 is the particle velocity only due to the incoming wave, there is no diffraction effects accounted for, unlike in the theory of *MacCamy* and *Fuchs* [35.44] based on the linear potential theory. The justification for this is that the diffraction effects are small because the cylinder is *slender*; therefore, u_1 and $\dot{u}_1$ are evaluated along the cylinder axis, since the errors made would be *small*.

Consider an oscillatory flow, in an *unbounded fluid* (no free surface or sea floor), with a period $T = 2\pi/\omega$, and velocity $u_1(t) = U\cos(\omega t)$, where U is the amplitude of velocity. The functional dependence of the force (per unit length) acting on the body, whose characteristic length is D, can be written as

$$\delta F = f(U, D, \rho, \nu, T) \,. \tag{35.68}$$

By applying dimensional analysis to (35.68), in which the set (ρ, U, D) is chosen as dimensionally independent, one can obtain

$$\frac{\delta F}{\frac{1}{2}\rho D U^2} = C_\mathrm{d}\left(\frac{UD}{\nu}, \frac{UT}{D}\right) , \tag{35.69}$$

or for the total force,

$$\frac{F}{\frac{1}{2}\rho D^2 U^2} = C_\mathrm{d}(\mathrm{Re}, \mathrm{KC}) , \tag{35.70}$$

where $\mathrm{Re} = UD/\nu$ is the usual diameter-based Reynolds number, and $\mathrm{KC} = UT/D$ is called the Keulegan–Carpenter(KC) number [35.45]. For large values of the KC number, $\mathrm{KC} \gg 1$, we expect the force coefficient, C_d, in (35.70) to approach the value of the steady (form-)drag coefficient, since large KC numbers correspond to long periods. In other words

$$C_\mathrm{d}(\mathrm{Re}, \mathrm{KC}) \to C_\mathrm{d}(\mathrm{Re}) \quad \text{if} \quad \mathrm{KC} \gg 1 . \tag{35.71}$$

On the other hand, when $\mathrm{KC} \ll 1$, the inertia effects will dominate viscous effects since the end of the time duration necessary to develop the boundary layer and flow separation could not have been reached. Therefore, we have basically an inviscid fluid since $\mathrm{Re} \to \infty$, or

$$C_\mathrm{d}(\mathrm{Re}, \mathrm{KC}) \to C_\mathrm{d}(\mathrm{KC}), \quad \mathrm{Re} \gg 1, \quad \mathrm{KC} \ll 1 . \tag{35.72}$$

If we now consider the presence of a *periodic free surface*, we can then anticipate that the force depends on

$$F = f(h, H, \lambda, D, \rho, \mathrm{g}, \nu) , \tag{35.73}$$

where h is the water depth, λ is the wavelength, and H is the wave height. In fact, it should not be difficult to obtain

$$\frac{F}{\rho \mathrm{g} H D^2} = f\left(\frac{h}{\lambda}, \frac{H}{\lambda}, \frac{D}{\lambda}, \mathrm{Re}\right) \tag{35.74}$$

by using dimensional analysis. If the problem is linear and the fluid is inviscid, we can write (35.74) as

$$\frac{F}{\rho \mathrm{g} H D^2} = f_1\left(\frac{D}{\lambda}, \frac{D}{h}\right) . \tag{35.75}$$

Therefore, if the fluid is inviscid, the force coefficient given in (35.74) does depend only on the ratio D/λ for a fixed-body geometry and water depth, that is, D/h is constant. So that $F = F(\omega)$ only, where ω is the angular wave frequency related to the wavelength through the linear dispersion relation. If we had explicitly included the frequency (or period) in the equations above, the KC number would also appear.

To see the effect of body dimension, wave height, and wavelength on the forces on a vertical, circular cylinder, consider Fig. 35.6. We see that as D/λ becomes small, the viscous effects (i. e., separation) become important. For a circular cylinder, and if $D/\lambda > 0.15$, the diffraction effects are more important. The KC number given in Fig. 35.6 is

$$K \equiv \mathrm{KC} = \frac{\pi H/\lambda}{\frac{D}{\lambda}\tanh(kh)} , \tag{35.76}$$

and it is evaluated at the still-water level and is for finite water depth. In infinite water, (35.76) becomes $\mathrm{KC} = \pi H/D$, since $\tanh kh \to 1.0$. Also, one can deduce from Fig. 35.6 that if $H/D > 1$, the viscous effects become important for a fixed ratio of D/λ. Therefore, in engineering calculations, it is recommended that, for a vertical circular cylinder that extends to the sea floor:

- If $\frac{H}{D} < 1.0$ and $\frac{D}{\lambda} \geq 0.15$, diffraction theory be used
- If $\frac{H}{D} \geq 1.0$ and $\frac{D}{\lambda} < 0.15$, Morison's equation be used.

It is noted that these should be cautiously used for other body geometries. In Fig. 35.6, $(H/\lambda)_{\max}$ is the maximum wave steepness (before wave breaking occurs) given by (for finite but large meaning not shallow-water depth, h)

$$\frac{H}{\lambda} = 0.14 \tanh(kh) . \tag{35.77}$$

In deep water, this clearly becomes $H/\lambda = 0.14$.

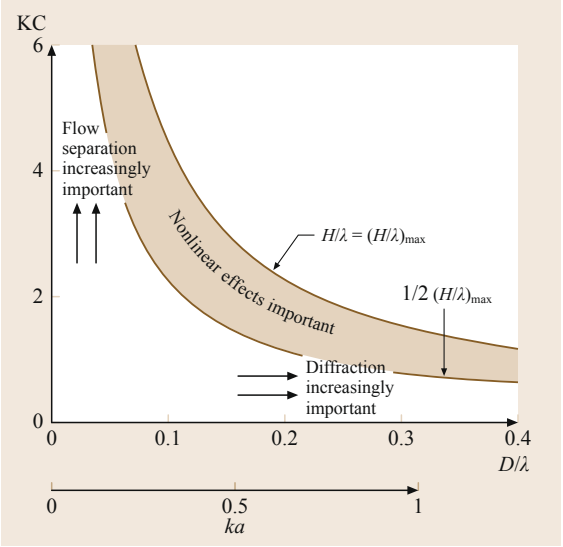

Fig. 35.6 Different wave force regimes (after [35.46])

Morison's equation is obtained by summing the inertia and drag terms. There can be no rational basis for this summation, especially since the coefficients C_a and C_d are intended to be constants and it can be shown easily that the $(1 + C_a)$ term is nothing but the sum of the Froude–Krylov force and the virtual mass force, that both can be obtained through the inviscid fluid and irrotational flow assumptions. In reality, the inertia and drag coefficients are also functions of the wave frequency. However, this formula is widely used in offshore and coastal engineering to determine wave and current forces on slender cylinders, such as drilling risers or jetty piles, and rather successfully.

Clearly, the drag term is nonlinear. This causes a slight problem in using Morison's equation, especially when the body is freely floating since the location where u_1 is calculated is unknown, and one must use the total *relative velocity* rather than u_1 alone if the body is freely floating. To overcome this problem, and also, to be consistent with the assumption of linearity, the drag term is linearized by defining a linear drag coefficient. There is one more reason for linearizing the drag force, and it is related to the use of spectral analysis in irregular waves which require that the system be linear.

To turn to the question of the linear drag coefficient, we write the horizontal component of the particle velocity as

$$u_1 = u_0 \cos(\omega t) \quad \text{at } x_1 = 0\,, \tag{35.78}$$

where u_0 is the amplitude of the velocity. The drag force in the direction of wave motion becomes

$$\delta F_d = \frac{1}{2}\rho D C_d u_0^2 \cos(\omega t)|\cos(\omega t)|\,. \tag{35.79}$$

The linear drag force can now be defined by equating the net work done (on a differential cylinder element) by the drag force δF_d, given by (35.79), and the linearized drag force, given by

$$\delta F_{dL} = \frac{1}{2}\rho D C_{dL} u_0 \cos(\omega t)\,. \tag{35.80}$$

This means that the viscous energy dissipated (per wave cycle) is the same whether we use (35.79) or (35.80). Therefore, by requiring equal energy dissipation per wave cycle, we must have $E_d = E_{dL}$

$$E_d = \int_0^\lambda \frac{1}{2}\rho C_d D u_0^2 \cos(\omega t)|\cos(\omega t)|\,\mathrm{d}x_1$$

$$= E_{dL} = \int_0^\lambda \frac{1}{2}\rho C_{dL} D u_0 \cos(\omega t)\,\mathrm{d}x_1\,. \tag{35.81}$$

Recalling also that $u_1 = \mathrm{d}x_1/\mathrm{d}t$ or $\mathrm{d}x_1 = u_0\cos(\omega t)\mathrm{d}t$, and $|\cos(\omega t)|\cos(\omega t) = \cos^2(\omega t)$ if $0 \le t \le T/4$, and that the total energy is equal to four times the energy per quarter of a wavelength for constants C_d and C_{dL}, we obtain, from (35.81)

$$C_{dL} = C_d \frac{\int_0^{T/4} u_0^3 \cos^3(\omega t)\mathrm{d}t}{\int_0^{T/4} u_0^2 \cos^2(\omega t)\mathrm{d}t} = \frac{8}{3\pi} C_d\, u_0\,. \tag{35.82}$$

Note that C_{dL} has the dimension of velocity, unlike C_d (which is dimensionless).

The amplitude of the horizontal velocity, u_0, is given, in linear potential theory, by

$$u_0 = \frac{gAk}{\omega}\frac{\cosh[k(x_2 + h)]}{\cosh(kh)}\,. \tag{35.83}$$

Substituting (35.82) into (35.80), we obtain

$$\delta F_{dL} = \frac{4}{3\pi}\rho D C_d u_0^2 \cos(\omega t)\,. \tag{35.84}$$

We need to note that there are other methods of linearization of the drag term, different from the method discussed here. Also, see [35.47–49] on the linearization of the drag force when a current is present, and when the waves are random.

There may also be current in the vicinity of the cylinder. Let us denote the steady shear-current velocity by $u_c = u_c(x_2)$. Also, it is possible that the cylinder is moving. In the case of a cylinder that extends to the sea floor, the only possible mode of motion is in the horizontal plane, $x_1 - x_3$, and this is called surging. However, Morison's equation is used not only to determine the forces on fixed platforms, such as

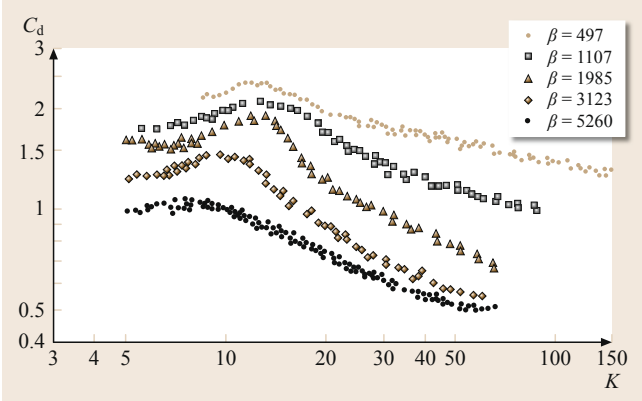

Fig. 35.7 Drag coefficient for a smooth circular cylinder as a function of the Reynolds and Keulegan–Carpenter numbers (after [35.51])

jack-up rigs, but also on floating platforms, such as semi-submersibles, which may have tubular structural members, such as columns, pontoons, or braces. These members may also be inclined, rather than just be vertical or horizontal. Therefore, in general, one can have three translational and three rotational (or angular) velocity components for the structure motion. In such cases, the velocity calculated in (35.67) must be the relative velocity

$$u_r = u_p + u_c - u_b \,, \tag{35.85}$$

where u_r is the relative velocity, u_p is the particle velocity, u_c is the current velocity, and u_b is the body velocity.

Drag and Inertia Coefficients

There have been many experimental studies on the drag and inertia coefficients used in Morison's equation. The most comprehensive references on the subject are the two monographs, [35.5] and [35.50]; they cite almost all previous experimental works on the inertia and drag coefficients. For example, [35.51] gives Figs. 35.7 and 35.8 for the drag and inertia coefficients, respectively, for smooth cylinders that were tested in a U-tube water tunnel as functions of the KC number and $\beta = \mathrm{Re}/\mathrm{KC}$, where KC is the Keulegan–Carpenter number and Re is the Reynolds number (Sect. 35.1.6).

A number of organizations also publish their recommended coefficients, For example, [35.52] recommends the following drag and inertia coefficients ($C_A = C_m - 1$) shown in Figs. 35.9 and 35.10

Some other organizations that recommend the use of certain coefficients are American Petroleum Institute, American Bureau of Shipping and Society of Naval Architects and Marine Engineers, and many other classified organizations whose publications are frequently referenced by regulatory agencies.

Viscous Drift Loads

Viscous drift forces originate mainly due to the existence of the drag force over the instantaneous submerged length of the members of platforms, due to the presence of current, and due to wave–current interaction effects. Traditionally, these forces have been computed using the drag force term of Morison's equation [35.43] to determine the mean forces and moments. Most of the studies on viscous drift forces prior to 1995 concentrated on analytical and/or experimental results for a single circular cylinder. For example, *Chakrabarti* [35.53] presented analytical expressions for viscous and potential drift forces on a vertical cylinder and compared the predictions with experimental data. The relative importance of the viscous and potential drift contributions has also been discussed.

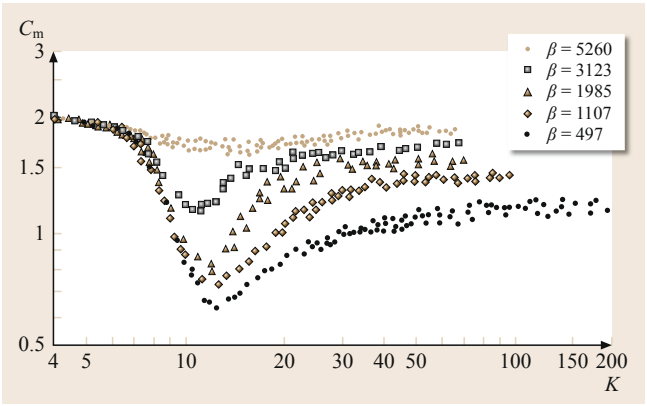

Fig. 35.8 Inertia coefficient for a smooth circular cylinder as a function of the Reynolds and Keulegan–Carpenter numbers (after [35.51])

Burns [35.54] used the relative velocity model of Morison's equation where the platform motion in surge is considered in determining the total relative velocity between the body and fluid. A method to obtain nonlinear viscous drift force transfer functions that can be used to determine the mean and slowly varying surge drift forces in irregular seas has also been presented. Other studies of viscous drift forces on the tension leg platform (TLP) [35.55] were also limited to the analysis of surge drift forces and motions. *Ertekin* and *Chitrapu* [35.56] computed the wave- and current-induced viscous drift forces and moments in all six degrees of freedom of a TLP. In that study, as well as in [35.57], first-order motions of the platform in all six degrees of freedom, given by the

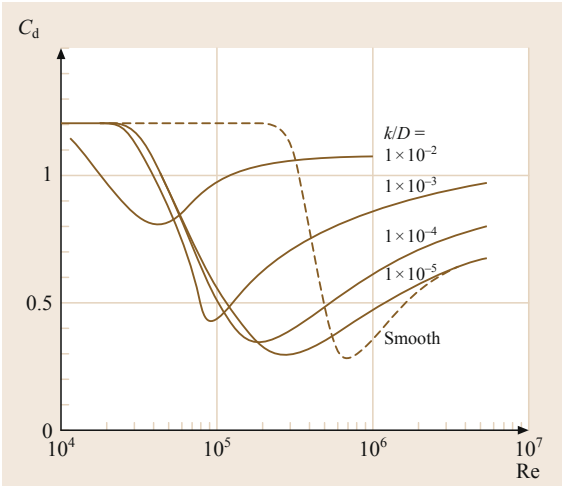

Fig. 35.9 Drag coefficient for a circular cylinder as a function of the roughness coefficient and Reynolds number (after [35.52])

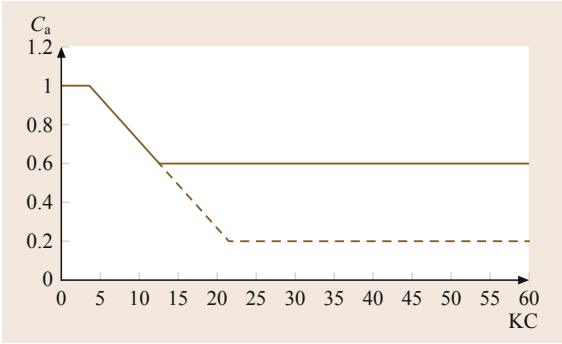

Fig. 35.10 Inertia coefficient for a circular cylinder as a function of the Keulegan–Carpenter number; *solid line* smooth cylinder and *dotted line* rough cylinder (after [35.52])

frequency-domain motion transfer functions are used to calculate the body velocity, and the resulting relative velocity is used to compute the drift forces and moments.

The evaluation of viscous drift forces in irregular waves is complicated due to the fact that the drift force is a nonlinear function of the wave height. From the results obtained in regular wave analysis, it appears that the viscous drift force, in the presence of current, is proportional to the third power of the wave amplitude as compared to the potential drift force which is proportional to the wave amplitude squared. Suitable methods have been developed to obtain potential drift forces in irregular waves using the regular wave results in conjunction with spectral analysis methods. The alternative is to use a time-domain method in which all nonlinearities can be included. However, frequency-domain methods for the computation of viscous drift forces in irregular waves are preferred in the preliminary design stage since they are computationally more efficient, although time-domain analysis is indispensable for the final design purpose [35.17, 57]. For this reason, several investigations are being carried out to develop frequency-domain methods for computing viscous drift forces in irregular waves [35.58, 59].

35.2 Current Loads

For the purpose of offshore engineering, it is the horizontal current that is of interest. Currents are important for vessel anchoring, installation work, riser interference, and vortex-induced vibration (VIV). Surface and mid-depth currents cause in-line and transverse forces on fixed and floating structures. Sea-floor currents may cause scour around structures and pipelines. This scour may compromise structural foundations or create unsupported spans in pipelines. The bottom current may also induce VIV in the unsupported spans of pipelines.

There are many components of the current in the ocean. Some of these currents extend to depths of several thousand meters and are poorly understood. Current types include:

1. Tidal currents
2. Wind driven
3. Ocean circulation
4. Boundary currents including loop and eddy currents
5. Internal waves and solitons.

The superposition of these current components generates the total current which can be represented by a current profile which gives speed and direction as a function of depth.

Currents are generally considered time invariant for purposes of offshore structure design, though in most cases, they comprise turbulent flow and vary in speed and direction with time. Currents are usually characterized by averages of the horizontal current vector over several minutes. Figure 35.11 illustrates how currents may vary in direction and magnitude at different depths and with time.

A description of currents should include the general circulation pattern in the area, tidal currents, and wind-driven currents. In most parts of the world, there is scarce current data because of the expense and the need for long-term observations required to capture a reasonable number of severe events. Yet design, planning for installation, and operation require information regarding the frequency of occurrence and seasonal variations of the current speed and direction. Whenever possible, site-specific measurements should be obtained throughout the water column and over sufficient time to capture several major events. When current models are used in lieu of site-specific measurements, the model should be validated against nearby measured data.

For design purposes, sufficient current information should be gathered to permit an estimate of the 100 year (1% annual probability of exceedance) event.

35.2.1 Nonuniform Currents

Current is rarely uniform with depth. Current profiles are frequently modeled as piecewise linear functions with the profile described in a table of depth, speed, and direction. Simple profiles, such as a uniform cur-

rent near the surface and zero elsewhere in the water column, are often used for design. Frequently, directional variation with depth is ignored or simplified for the purpose of design calculations. These simplifications are used when the simplification is conservative and yet does not appear to increase cost unreasonably.

The currents in a region will be a function of the local topography and oceanography, including density distribution and the flow into or out of the area (Fig. 35.12). Shallow-water currents are frequently driven by tides, and simple profiles of speed versus depth provide an adequate description. Deepwater currents as illustrated in Fig. 35.11 can vary greatly in the speed and direction with depth and may require a more complex description.

Shallow-water and near-bottom currents will often exhibit a power-law profile, such as given by (35.86).

$$U_c(z) = U_{c0}\left(\frac{z+h}{h}\right)^{\alpha} , \qquad (35.86)$$

where $U_c(z)$ is the current speed at elevation z, where $z = 0$ at the surface; U_{c0} is the surface current speed; h is the water depth; α is an exponent (typically $1/7$).

A method for developing design current profiles from long-term measured current profile data sets is described in [35.62]. The data are parameterized using empirical orthogonal functions, and then the design current profile with the required return period is selected through a process involving an inverse first-order reliability method (FORM).

35.2.2 Wave–Current Interaction

When waves propagate on a current, the encounter frequency of the wave encountering a fixed body is different from the intrinsic frequency of the waves. It is the intrinsic frequency that determines the wavelength and the wave kinematics. Much wave data are collected from fixed platforms that measure the encounter frequency. This fixed platform data must be corrected to the intrinsic frequency since wave spectra for criteria are usually represented in terms of the intrinsic frequency.

For an effective current speed U, moving in the same direction as the waves, the encounter wave frequency is higher than the wave frequency alone. The encounter frequency is $\omega_A = 2\pi/T_A$, where T_A is the encounter period seen by a fixed observer. The two frequencies are related by the Doppler shift as

$$\omega = \omega_A - kU , \qquad (35.87)$$

where k is the wave number and ω is the intrinsic frequency. The last term in (35.87) is called the convective frequency. The Doppler effect is computed based on the component of the ambient current in the direction of

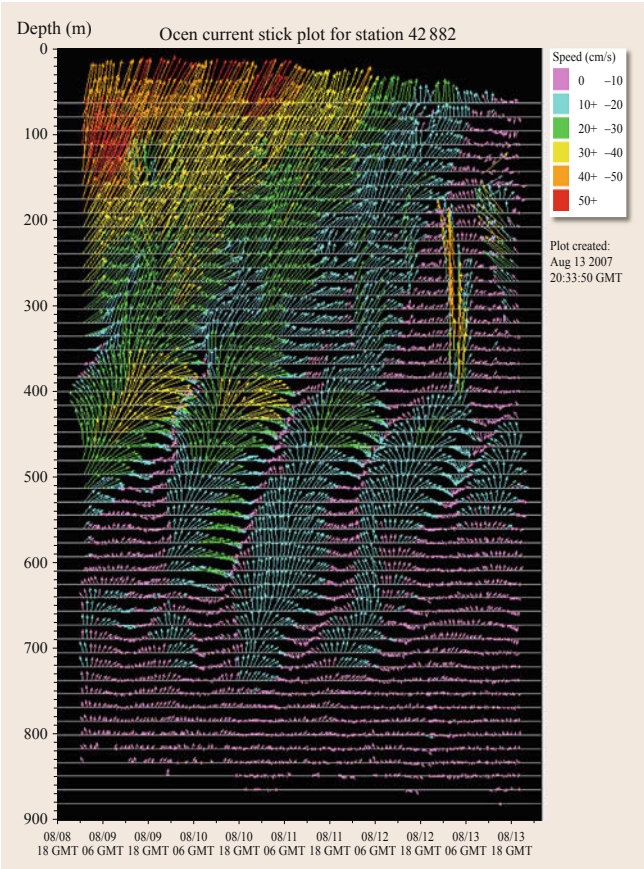

Fig. 35.11 National Data Buoy Center (NDBC) stick plot of currents acquired by oil and gas companies in the northern Gulf of Mexico (after [35.60])

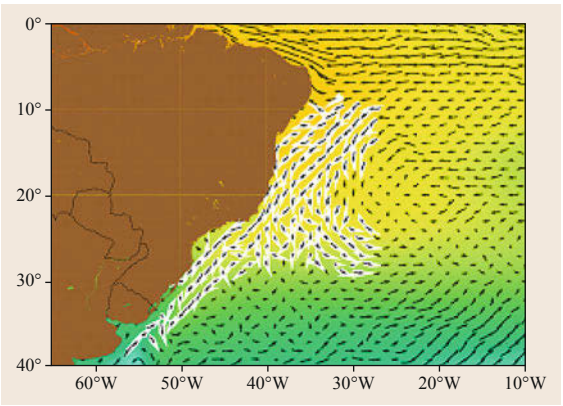

Fig. 35.12 The Brazil current as represented by the Mariano Global Surface Velocity Analysis (MGSVA) (after [35.61])

waves U. If the current profile is not uniform, *Kirby* and *Chen* [35.63] showed that the encounter wave period is computed from (35.87) and the following equations

$$\omega^2 = gk \tanh(kh) \,. \tag{35.88}$$

$$U = \frac{2k}{\sinh 2kh} \int_{-h}^{0} U_c(z) \cosh[2k\,(z+h)]\,\mathrm{d}z \,, \tag{35.89}$$

where h is the water depth and $U_c(z)$ is the current profile.

The frequency parameter in wave spectra formulations (Sect. 35.1.4) is the intrinsic frequency. A fixed or floating stationary structure in a wave field with current responds to the encounter frequency rather than to the intrinsic frequency. For wave-response calculations, the wave-frequency spectrum should be transformed into the encounter frequency. The wave energy per frequency band is independent of the reference frame so that $S(\omega)\,\mathrm{d}\omega = S(\omega_A)\,\mathrm{d}\omega_A$. Equation (35.87) is used to make the frequency transformation, where the wave number k is a function of the intrinsic wave frequency ω through (35.88).

35.2.3 Wave Current Kinematics

The kinematics of waves propagating through a uniform current can be modeled simply by adding the current vector to the wave velocity vector. When the current profile varies significantly through the wave zone, this simple model does not apply. Several approximations have been put forward to model the combined regular wave and current velocity. These approximations are extensions of the same approximations used to estimate wave kinematics near the free surface when no current is present.

A current profile is defined from the mean water line to the bottom. Waves change the location of the free surface and transform the current profile as they pass [35.64, 65].

A linear transformation of the current profile incorporates a stretching factor F_s

$$F_s = \frac{\eta + h}{h} \,, \tag{35.90}$$

where η is the water-surface elevation measured upward from the still-water level and h is the still-water depth.

The transformed current beneath the instantaneous water surface is $U_c\left(\frac{h+z_s}{F_s} - h\right)$, where z_s is the elevation measured upward from the still-water level and $U_c(z)$ is the current profile absent waves. A linearly stretched current profile is exactly analogous to the stretching of linear wave kinematics as applied by [35.66].

The nonlinear transformed current at an elevation z_s is $U_c(z)$, where z is determined by solving

$$z_s = z + \eta \frac{\sinh(k_{nl}(z+h))}{\sinh(k_{nl}h)} \,, \tag{35.91}$$

where k_{nl} is the wave number for the regular wave under consideration for water depth h, crest elevation η, and the intrinsic wave frequency ω. k_{nl} is calculated using the dispersion relationship of the nonlinear wave theory being used.

A simple modification of the nonlinear regular wave method described above can be used for random waves. In this case, the wave period and length correspond to the period and length of the spectral peak frequency.

Once the current profile is transformed to correspond to the instantaneous wave, the total horizontal water velocity at an elevation is the sum of the current vector and the wave velocity vector at that elevation.

35.2.4 Current-Induced Forces

Forces induced by currents on offshore structures are usually modeled as constant. These forces are nonlinear and, thus, the interaction with waves and with structure motions must be considered. The members of a structure in a steady flow experience a drag force proportional to the square of the flow velocity

$$f = \frac{1}{2}\rho U^2 A C_d \,, \tag{35.92}$$

where ρ is the mass density of the fluid, U is the flow velocity, A is the area of the member, and C_d is the drag coefficient. The drag coefficient is a function of the Reynolds number (Re) and the relative roughness of the surface (e) (Sect. 35.1.6).

This same drag force is a component of the force on a member in the oscillating flow, in waves calculated using the Morison equation (Sect. 35.1.3). In oscillating flows the drag coefficient is also a function of the Keulegan–Carpenter(KC) number already discussed in Sect. 35.1.3. Note also that the combination of the steady-current velocity and the oscillating wave-induced velocity causes an increase in the average drag force on a body due to the quadratic nonlinearity of the drag term in the Morison equation.

A current also induces a nonlinear time-varying force transverse to the direction of the current known as the lift force

$$f_L = \frac{1}{2}\rho U^2 A C_L \,, \tag{35.93}$$

where C_L is the lift coefficient. The lift force even in a steady flow is time varying. Thus, the lift coefficient reflects the RMS lift force or the maximum lift force over a period encompassing a number of oscillations of the lift force. These transverse forces are also referred to as vortex-induced forces and can cause large deflections of slender members free to vibrate known as VIV or large deflections of flexible structures known as vortex-induced motion (VIM) when the shedding period of vortices in the wake of the structure is close to natural periods of structure vibration. The shedding of vortices in the wake of a body also induces unsteady forces in line with the current direction. These unsteady inline forces are generally smaller than the transverse forces and much smaller than the average inline current force. The unsteady inline forces usually occur at twice the frequency of the transverse forces but can induce significant motions when they occur at a frequency close to the natural frequency of vibration of the structure.

Structures which appear transparent to currents can induce significant current blockage. The structure causes some of the current to go around the structure rather than through it. Current flows through these structures at a reduced velocity. Accounting for the reduced currents may be of interest for the design structures, especially when they accommodate a large number of conductors or risers. Current speed reduction factors ranging between 7 and 9 for jacket-type structures are provided in [35.67]. These factors are applied to the undisturbed current profile to obtain the current to use in force calculations.

The wake of an object located within a few diameters upstream of another object will influence the forces on the downstream object. Shielding will reduce the drag force on the downstream object and shear in the wake will induce lift forces on the downstream object. The drag and lift forces will depend on the spacing of the objects. The average current speed U_w in the turbulent wake of a cylinder at a point x downstream and y transverse to the current per [35.68] is

$$U_w = U - k_2 U \sqrt{\frac{C_d D}{x_s}} e^{-0.693\left(\frac{y}{b}\right)^2}, \tag{35.94}$$

$$x_s = x + \frac{4D}{C_d}, \tag{35.95}$$

$$b = k_1 \sqrt{C_d D x_s}, \tag{35.96}$$

where the empirical coefficient $k_1 = 0.25$ and coefficient $k_2 = 1.0$, and D is the upstream cylinder diameter and C_d is the upstream cylinder drag coefficient. This current in the wake is used to calculate the drag force on the downstream object.

The shielding may be beneficial in that it reduces forces on the downstream object, or it may be detrimental if the reduced forces lead to reduced distance between the objects which leads to clashing. This clashing is of particular concern for closely spaced risers in deep water.

For configurations comprising multiple closely spaced cylinders, experimental data possibly supported by computational fluid dynamics (CFD) should be used. Otherwise, interference effects should be ignored where beneficial and experiments should be considered where clashing is a concern.

Forces due to currents are calculated using the Morison equation (Sect. 35.1.6). The superposition of current and wave velocities should be considered when the local amplitude of the wave-induced water motion is larger than the radius of the member under consideration. The current vector and wave particle velocity vector should be added before the force is computed. Due to the nonlinear nature of the drag force in the Morison equation, currents can affect dynamic forces and should thus be modeled when dynamics is important.

35.2.5 Vortex-Induced Vibrations

VIVs can be caused by the flow of any fluid past a structure. Vortices are shed in the wake of the structure causing force transverse to the direction of the flow which may cause motions transverse to the flow which in turn may reinforce the vortex shedding. This may lead to large oscillations particularly in long slender elements normal to their long axis.

Parameters that influence these VIVs include: slenderness (L/D), mass ratio ($m^* = m/\left(\frac{1}{4}\pi\rho D^2\right)$), damping ration ($\zeta$), Reynolds number ($\mathrm{Re} = UD/\nu$), reduced velocity ($V_R = U/f_n D$), and flow properties, such as oscillations, turbulence (σ_U/U), and profile, where L is the member length, D is the member diameter, m is the mass per unit length, ζ is the ratio between damping and critical damping, ρ is the fluid density, ν is the fluid kinematic viscosity, U is the mean fluid speed, f_n is the natural frequency of the member, and σ_U is the standard deviation of the flow speed.

For the steady flow, the vortex shedding frequency is

$$f_s = \mathrm{St}\frac{U}{D}, \tag{35.97}$$

where St is the Strouhal number. For a smooth fixed circular cylinder in the steady flow, the Strouhal number is a function of the Reynolds number as shown in Fig. 35.13.

Table 35.2 Efficiency of helical strakes and helical wires (after [35.52])

	Number of windings	Height of strakes	Pitch	Lift coefficient C_L	Drag coefficient C_d
Helical strakes	3	.11D	4.5D	0.238	1.6
	3	.11D	15D	0.124	1.7
Helical wires	3–4	.118D	5D	0.2	1.17
	3–4	.118D	10D	0.2	1.38
No spoilers				0.9	0.7

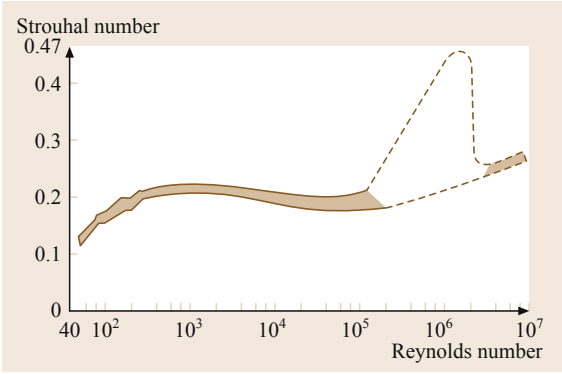

Fig. 35.13 Strouhal number for a circular cylinder as a function of the Reynolds number (after [35.69])

When the vortex shedding frequency coincides with natural frequencies of vibration, large-amplitude motions may arise. This phenomenon is called lock-in because the motions and vortex shedding will occur at the natural frequency of the body over a range of flow speed. The natural frequency of the body may be different from that observed in still water due to flow-induced variation in added mass. Lock-in can occur in line with the flow as well as transverse to the flow. Lock-in occurs when the reduced velocity V_R is close to the inverse of the Strouhal number.

The mass ratio m^* is an indication of the relative importance of the body mass and the fluid forces. A high mass ratio indicates that the fluid force is relatively small compared to the body inertia. For situations with a low mass ratio, such as a pipe in water, the lock-in range is $3 < V_R < 16$ and for a high mass ratio, such as wire in air, the lock-in range is $4 < V_R < 8$.

VIV on a slender member will cause fatigue damage, may increase the drag coefficient of the member causing additional load and possibly clashing, and may excite vibration and VIV of downstream objects.

The responses of structures to flow-induced vibrations can be estimated via model tests, response-based methods, force-based methods, or flow-based methods. Response-based methods [35.70, 71] estimate steady-state responses of systems as a function of structural and hydrodynamic parameters making use of conservative envelopes of experimental data. Force-based methods make use of a structural model excited by inertia and damping forces determined from empirical data. They attempt to model the flow explicitly and include CFD which solve the Navier–Stokes equations coupled with a structural model.

Vortex shedding may also induce motions in the hull of floating systems. These motions are important because these motions can influence mooring and riser design. Cross-flow oscillations are generally larger than inline oscillations and are, thus, of most interest. For large circular cylinders, like Spars, the amplitude of VIMs can be up to 80% of the diameter. This can be reduced to 40% or less with suppression devices. Model tests are generally used to estimate the motions of these structures with and without suppression devices.

The suppression of VIV is generally done with devices which spoil the wake and reduce the coherence of vortex shedding along the structure. This can be done with fins which weather a vane and help keep the wake symmetric and reduce the size of shed vortices. The wake can also be spoiled by making the member irregular along its length by wrapping it with helical strakes or wires (Table 35.2).

35.3 Wind Loads

Offshore platforms are exposed to wind fields which pose a serious overload threat to the overall platform structural system as well as to topside components, such as helidecks, drilling derricks, cranes, and living quarters. Fluctuating wind loads as well as VIVs can cause fatigue damage and lead to failures. Reliable design to resist these failure mechanisms requires a good understanding of the wind environment and as well as the mechanisms of wind loading.

The wind speed and direction vary in space and time. Sufficient data to describe the spatial and time variations in a great detail are rarely available and for most applications are unnecessary. Wind field descriptions are based on statistical parameters, such as the

mean and the standard deviation of the speed, as well as the mean direction. Both length scales and time scales influence the definition of these statistical parameters.

Both local and global wind effects on platforms must be considered. The local effects influence the design of the deck structure and equipment. Global effects, such as overturning moments and total lateral loads, drive the design of foundations and mooring systems. Both mean and fluctuating forces must be considered. Compliant structures such as TLPs have natural frequencies of motion in the horizontal plane which can be excited by wind forces and make them sensitive to the slowly varying fluctuations of the wind.

Extreme and normal wind conditions should be specified when designing offshore structures. The response of the structure to wind will influence which conditions are of interest. Three-dimensional spatial scales of wind are related to the durations of turbulent gusts. Thus, gusts of a few seconds duration will have less influence on a large structure than will gusts of a minute duration. The time variation of the wind, usually characterized by a spectrum, should be considered for structures with appreciable dynamic response.

A description of the wind environment for a location should include an estimate of extreme wind speeds in specified directions and specified averaging times as a function of the recurrence interval. Information about the measurement sites and a description of the measured data used to generate the environment description should be available. The frequency of exceedance of specified thresholds from specified directions during the service life should be estimated. The types of storms causing high winds should be described. Similar information should be provided for normal or short-term conditions providing descriptions by month or season. Figure 35.14 is an example of such a monthly description.

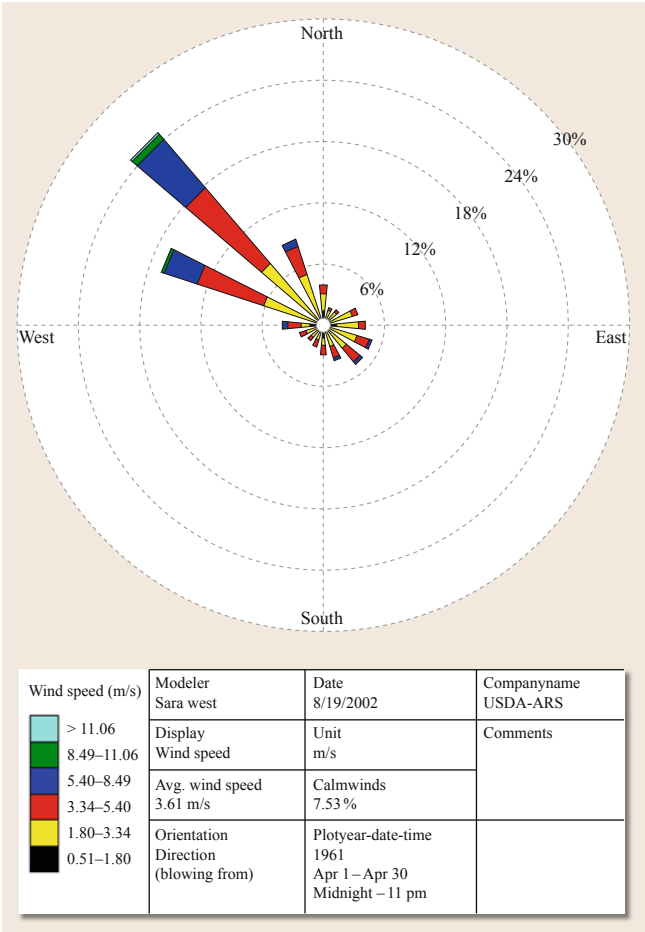

Fig. 35.14 Wind rose showing the statistical variation of wind direction and speed during the month. The length of each *line* indicates the percentage of time the wind blew from that direction during the month. The *colors* indicate different wind-speed bins (after [35.72])

35.3.1 Wind-Speed Profile

On length scales typical of even the largest offshore structures, the mean and standard deviation of the wind speed, averaged over durations of the order of an hour, do not vary horizontally, but they do change with elevation. For averaging durations shorter than an hour, there will be periods with higher mean speeds and the spatial variations will increase. To be meaningful, a wind-speed value must be qualified by an elevation and a duration over which it is averaged. An elevation of 10 m above the mean sea level is used as a standard reference height.

According to *Planning* [35.67], the mean wind-speed profile $U_w(z)$ under storm conditions can be more accurately described by a logarithmic profile as given in (35.98) than by the traditional power-law profile

$$U_{w,1h}(z) = U_{w0}\,[1 + C \ln (z/z_r)\,]\,, \qquad (35.98)$$

where $U_{w,1h}(z)$ is the 1 hour sustained wind speed at a height z above the mean sea level; U_{w0} is the 1 hour sustained wind speed at the reference elevation z_r and is the standard reference speed for sustained winds; C is a dimensionless coefficient, the value of which is dependent on the reference elevation and the wind speed, U_{w0}. For $z_r = 10\,\text{m}$, $C = 0.0573\sqrt{1 + 0.15U_{w0}}$, where U_{w0} is in units of meters per second (m/s); z is the height above the mean sea level; and z_r is the reference elevation above the mean sea level ($z_r = 10\,\text{m}$).

For the same conditions, the mean wind speed for averaging times shorter than 1 hour may be expressed

by (35.99) using the 1 hour sustained wind speed $U_{w,1h}(z)$ of (35.98)

$$U_{w,T}(z) = U_{w,1h}(z)\left[1 - 0.41 I_u(z) \ln\left(\frac{T}{T_0}\right)\right], \tag{35.99}$$

where $U_{w,T}(z)$ is the sustained wind speed at height z above mean sea level, averaged over a time interval $T < 3600\,\mathrm{s}$; $U_{w,1h}(z)$ is the 1 hour sustained wind speed at height z above mean sea level, see (35.98); T is the time-averaging interval with $T < T_0 = 3600\,\mathrm{s}$; T_0 is the standard reference time-averaging interval for the wind speed of $1\,\mathrm{h} = 3600\,\mathrm{s}$; $I_u(z)$ is the dimensionless wind turbulence intensity at a height z above the mean sea level, given by (35.100), where U_{w0} is in m/s

$$I_u(z) = 0.06\,(1 + 0.043 U_{w0})\left(\frac{z}{z_r}\right)^{-0.22}. \tag{35.100}$$

Note that the equations in this section are derived from curve fitting through available data [35.73] and contain numerical constants that are only valid in the SI units of meters and seconds. The above equations are not valid for the description of winds in short-lived events, such as squalls and tornados, since the duration is often less than 1 hour. Adjustments to the wind profile at a particular location or under certain conditions can be made when specific appropriate measured data from an offshore location are available (i. e., measured data for the kind of event used in design).

35.3.2 Wind Spectra and Gusts

The wind spectrum characterizes the time-varying properties of the wind. These variations are due to boundary-layer turbulence which depends on the wind speed and the thermal stability of the air. The following wind spectrum formulation is based on measurements under conditions of nearly neutral thermal stability as documented in [35.73].

Equation (35.101) describes the spectrum of wind speed at a point in space and is analogous to the spectra used to describe the time-varying kinematics of waves in Sect. 35.1.4.

$$S(f,z) = \frac{320\left(\frac{U_{w0}}{U_{ref}}\right)^2\left(\frac{z}{z_r}\right)^{.45}}{\left(1+\tilde{f}^n\right)^{5/(3n)}}, \tag{35.101}$$

where $S(f,z)$ is the wind spectrum (spectral or energy density function) at frequency f and elevation z in m^2/s; U_{w0} is the 1 h sustained wind speed at the reference elevation z_r (the standard reference speed for sustained winds); U_{ref} is the reference wind speed, $U_{ref} = 10\,\mathrm{m/s}$; f is the frequency in cycles per second (hertz) over the range $0.00167\,\mathrm{Hz} < f < 0.5\,\mathrm{Hz}$; z is the height above the mean sea level; z_r is the reference elevation above the mean sea level ($z_r = 10\,\mathrm{m}$); $\tilde{f}$ is a non dimensional frequency defined by (35.102) where the numerical factor 172 has the unit of second (s)

$$\tilde{f} = 172 f\left(\frac{z}{z_r}\right)^{2/3}\left(\frac{U_{w0}}{U_{ref}}\right)^{-.75}. \tag{35.102}$$

n is a coefficient equal to 0.468.

Integrating the spectrum over the applicable frequency range yields the standard deviation of the wind speed. When comparing the spectrum to data, comparable frequency ranges should be used.

The spatial and temporal wind fields are correlated. Thus, the wind spectrum should be complemented with a description of the spatial coherence. It is generally conservative to assume that the wind speed is fully correlated over a complete structure. But it is reasonable to take advantage of the reduced correlation when estimating loads on structures. Equation (35.103) describes the coherence between two points P_1 and P_2, with positions in the wind directions of x_1 and x_2, and position transverse to the wind directions of y_1 and y_2, and elevations above the mean water of z_1 and z_2

$$F_{Coh}(f, P_1, P_2) = \exp\left[-\frac{1}{U_{w0}}\left(\sum_{i=1}^{3} {A_i}^2\right)^{1/2}\right], \tag{35.103}$$

where $F_{Coh}(f, P_1, P_2)$ is the coherence function between turbulence fluctuations at P_1 and at P_2; U_{w0} is the 1 hour sustained wind speed at 10 m above the mean sea level in meters per second (m/s); A_i is a function of frequency and the position with units of m/s calculated from (35.104)

$$A_i = \alpha_i f^{r_i} D_i^{q_i}\left(\frac{z_g}{z_r}\right)^{-p_i}, \tag{35.104}$$

where f is the frequency in Hertz (Hz), D_i is the distance, measured in meters (m), between points P_1 and P_2 in the x, y, and z directions for $i = 1, 2$, and 3, respectively (Table 35.3); z_g is the geometrical mean height of the two points, $z_g = \sqrt{z_1 z_2}$; z_r is the reference elevation above the mean sea level, $z_r = 10\,\mathrm{m}$; α_i, p_i, q_i, r_i are coefficients given in Table 35.3.

The concept of a wind spectrum is only applicable to steady wind conditions. The time and spatial variation of the wind speed in a squall or tornado cannot be described by a wind spectrum. The analysis of forces

Table 35.3 Coefficients in (35.103) for points P_1 and P_2

i	D_i	a_i	p_i	q_i	r_i
1	$\lvert x_1 - x_2 \rvert$	2.9	0.4	1.00	0.92
2	$\lvert y_1 - y_2 \rvert$	45.0	0.4	1.00	0.92
3	$\lvert z_1 - z_2 \rvert$	13.0	0.5	1.25	0.85

and responses caused by squalls and tornados requires the specification of a time series of wind velocity.

Wind speeds are frequently classified as sustained winds or gusts. Sustained winds are usually hourly averages and gusts are usually the hourly maxima of averages of a minute or less. In either case, the averaging duration should always be stated as well as the elevation. The duration of interest depends on the dimensions and natural period of the structure being analyzed. Small structures should be designed for a shorter gust duration (and hence a higher gust wind speed) than a larger structure. Gusts naturally arise due to the turbulence in wind and can be considered local maxima rather than transient wind conditions. Gust wind speeds are generally derived from the wind spectrum.

Equation (35.99) may be used to calculate the gust speed for various gust durations. Squalls, thunderstorms, downbursts, tornados, and water spouts are relatively short-lived phenomena which can induce extreme winds. The ratio of the maximum gust wind speed to hourly mean wind speed at any one location in these examples can be large. Turbulence alone generates gusts during periods of high mean wind speed, but in this case the ratio of the maximum gust wind speed to hourly mean wind speed over the sea is typically less than about 1.5.

35.3.3 Steady-State Forces

For fixed structures, global wind forces are generally much less important than those caused by waves and currents. Wind forces on individual components of these structures can be significant, however. Global forces on structures are determined using a time-averaged wind speed in the form of a sustained wind speed. For the design of individual structural components, a time-averaged wind speed can also be adequate, but the averaging duration should be reduced to allow for the smaller turbulence scales that can affect individual components. The wind in a 3-s gust is appropriate for determining the maximum static wind load on individual members; 5-s gusts are appropriate for maximum total loads on structures whose maximum horizontal dimension is less than 50 m; and 15-s gusts are appropriate for the maximum total static wind load on larger structures.

Wind acts on a structure above the water, as well as on any equipment, deck houses, bridges, flare booms, and derricks that are located on the topsides. The height of the component above the sea level should be taken into account when estimating the wind speed.

Table 35.4 Wind shape coefficients

Area	Shape coefficient C_S
Beams	1.5
Sides of buildings	1.5
Cylindrical sections	0.5
Overall projected area of platform	1.0

Equation (35.99) can be used to calculate the gust speed for various gust durations for a given elevation z.

The steady wind pressure q is calculated as

$$q = \frac{1}{2}\rho U^2 \,. \tag{35.105}$$

And the force F, acting normal to the body axis or surface, is calculated as

$$F = qC_S A \sin\alpha \;\;, \tag{35.106}$$

where ρ is the density of air (1.22 kg/m^3 for standard temperature and pressure), U is the wind speed (m/s), A is the object area (m^2), α is the angle between the direction of the wind and the axis of the exposed member or surface, and C_S is the shape coefficient.

For smooth circular tubular structures, the shape coefficient is $C_S = 0.65$ for the Reynolds number $> 5 \times 10^5$, and $C_S = 1.2$ for the Reynolds number $< 5 \times 10^5$. A good collection of shape coefficients for long bodies and bodies of finite length is presented in [35.52]. Table 35.4 provides shape coefficients recommended in [35.67] for several bodies for the perpendicular wind approach angle.

On most structures, objects exposed to wind loads are closely spaced and shield each other from the wind depending on the wind direction. If a detailed model of the wind-loaded objects is used, shielding coefficients should be included to account for this interaction. Wake models similar to that presented in (35.94) can be used to estimate shielding.

Wind tunnel tests should be considered to determine pressures and resulting loads on complex structures. Testing should include the variation of wind speed with elevation as well as turbulence.

35.3.4 Unsteady Forces

Modeling the time and spatial variation of the wind should be considered for structures and components which respond dynamically to wind loads. A dynamic analysis of a structure is generally necessary when the wind field contains energy at frequencies near the natural vibration frequencies of the structure; this is

generally the case for compliant bottom-founded platforms as well as for floating structures. Time-varying wind forces can cause resonant surge, sway, and yaw motion of floating anchored structures.

Good load and response estimates can be obtained from boundary-layer wind tunnels and from CFD. Reasonable results can be obtained by simulating forces and responses using a time-domain synthesis of the wind spectrum, (35.101), and adding it to the mean wind. The spatial variation of the wind speed can also be modeled by making use of the coherence function (35.103).

The instantaneous wind force can be calculated by the summation of the forces on individual members exposed to wind. The pressure q can be estimated by

$$q = \frac{1}{2}\rho_a \left|U_{w,T} + u - \dot{x}\right| \left(U_{w,T} + u - \dot{x}\right) , \quad (35.107)$$

where $U_{w,T}$ is the mean wind velocity, u is the gust velocity which may vary spatially as well as with elevation, $\dot{x}$ is the velocity of the body, and ρ_a is the mass density of air ($1.226\,\mathrm{kg/m^3}$ for dry air at 15 °C).

When the structural velocity $\dot{x}$ is negligible compared to the wind speed, the wind pressure can be linearized to

$$q = \frac{1}{2}\rho_a {U_{w,T}}^2 + \rho_a U_{w,T} u . \quad (35.108)$$

These time-varying pressures can be used with (35.106) to calculate time-varying forces.

A special case of dynamic response is VIV of relatively slender structures subjected to steady winds in which alternate vortex shedding excites components. Components of fixed steel offshore structures can be exposed to wind VIV during construction and transportation. Flare structures and telecommunication towers can also be susceptible to wind VIV throughout their lives. Vortex shedding and VIV in wind are much the same as for currents. See Sec. 35.2.5 for a discussion of these phenomena.

35.4 Model Tests

Regardless of how good we think the theoretical predictions of a physical quantity is, there will always be errors, however small, due to the particular modeling we use, or errors in the numerical analysis we perform. We may also have truncation and round-off errors, not to mention any human errors that may be present. All these potential errors can be assessed in a comprehensive way by conducting model tests. However, one has to realize that model tests themselves are not necessarily free of potential errors either, mainly due to the fact that the tests are conducted in a rather finite domain that may be the cause of reflections from tank walls, the wavemaker and absorption beach(es) that in turn may contaminate the measured data.

Physical modeling is the most important area that dimensional analysis can be applied to. By physical modeling, we refer to the technique of reproducing a physical phenomenon on a greater or smaller scale. The motions of or the wave loads on offshore platforms that can be measured by means of model tests in a test basin are the examples to model testing at a smaller scale. There are two basic issues that need to be addressed in any model testing: 1) how do we conduct the experiments so that the data obtained at the model scale are accurate, and 2) how do we extrapolate the data to the prototype scale?

In most offshore engineering problems, the three dimensions, length (L), mass (M), and time (T), are the fundamental dimensions. All physical quantities can then be measured in terms of these three fundamental dimensions. However, some physical quantities, such as temperature and angle, may occasionally be used as one of the fundamental dimensions. If a measurement results in a real number, which can directly be compared to one of these fundamental dimensions, then the measurement is called a direct measurement. For example, a distance of 5 m is a direct measurement since its unit is one of the fundamental units, namely the length. On the other hand, if a measurement is a result of various comparisons that give a real number, whose dimension is a combination of two or more fundamental units, then the measurement is called a derived measurement. A typical example is the velocity, since both length and time have to be measured to obtain the velocity. In derived measurements, there is always a function that expresses the relation between the direct measurements. In the case of velocity measurements, for example, this function is $f(x,t) = \mathrm{d}x/\mathrm{d}t$.

35.4.1 Principles and Similarity Laws

The scale model of any prototype system has to satisfy certain conditions called the laws of similarity or similitude so that the behavior of the prototype phenomenon can accurately be reproduced. The similarity can refer to one or more of:

1. Geometric similarity (refers to length)
2. Kinematic similarity (refers to velocity)
3. Dynamic similarity (refers to force).

The wave loads or motions of offshore platforms or any other physical quantity of interest have to obey one or more of these similarity laws in order that one can properly conduct experiments [35.74].

It is necessary at this point to introduce various force mechanisms that are present in the flow of real fluids. This necessity arises because, under certain conditions of the specific problem being investigated, some force mechanisms may be dominant over the other. As a result, we may isolate, or even neglect, the smaller forces by choosing a proper similarity law. The three principal types of internal force mechanisms in a real fluid are:

1. Inertial force
2. Gravitational force, and
3. Viscous force.

The inertial force is due to the fluid particle acceleration and is proportional to $\rho u(\partial u/\partial x)$, where ρ is the fluid mass density, and u is the particle velocity component in the x direction (other terms are left out without loss of generality). The gravitational force is due to the weight of the fluid itself and is proportional to ρg, where g is the gravitational acceleration. The viscous force is due to the difference between the shear forces acting on a fluid element, and is proportional to $\mu\partial^2 u/\partial x^2$, where μ is the dynamic viscosity coefficient (again other terms are left out). All these forces are included in the Navier–Stokes equations.

The ratios of the internal forces (per unit volume) with one another give us the relative importance or dominance of these forces. For example, we can write the ratio of

$$\frac{\text{Inertial force}}{\text{Gravitational force}} \propto \frac{\rho u\frac{\partial u}{\partial x}}{\rho g} = \frac{u}{g}\frac{\partial u}{\partial x} \propto \frac{U^2}{g\ell} \,. \tag{35.109}$$

In (35.109), U is a characteristic velocity, ℓ is a characteristic length of the problem, and ρ and g are the fluid mass density and gravitational acceleration, respectively. It is seen that the ratio is proportional to $U^2/g\ell$. Similarly, we can write the ratio of

$$\frac{\text{Inertial force}}{\text{Viscous force}} \propto \frac{\rho u\frac{\partial u}{\partial x}}{\mu\frac{\partial^2 u}{\partial x^2}} \propto \frac{U\ell}{\upsilon} \,, \tag{35.110}$$

where $\upsilon = \mu/\rho$ is the kinematic viscosity coefficient. The third ratio, the ratio of the gravitational force to viscous force, can be obtained by a combination of (35.109) and (35.111), and, therefore, it need not be considered. The square root of (35.109) is the Froude number Fr and (35.110) itself is the Reynolds number Re. So, for small Fr, for instance, we can say that the flow is gravity dominated, and for large Re, for instance, we can say that the flow is inertia dominated or viscosity is negligible (or the inviscid fluid assumption is a good one).

If we require that the flow about a body be similar fully both in the model and prototype scales, then it is necessary that both the Fr and Re numbers be the same for the model and prototype. In other words, the Froude number of the model scale must be the same as the Froude number of the prototype scale, that is, $\mathrm{Fr_m} = \mathrm{Fr_p}$, and similarly for the Reynolds number, that is, $\mathrm{Re_m} = \mathrm{Re_p}$, where the subscripts m and p refer to the model and prototype, respectively. Unless under very special circumstances, it is not practically possible to scale a prototype by holding both the Fr and Re numbers the same. To see this, consider the Froude number and the Reynolds number, keeping both constant for the model and prototype scales, that is

$$\begin{aligned} \mathrm{Fr_m} &= \frac{U_\mathrm{m}}{\sqrt{g_\mathrm{m}\ell_\mathrm{m}}} = \mathrm{Fr_p} = \frac{U_\mathrm{p}}{\sqrt{g_\mathrm{p}\ell_\mathrm{p}}} \,, \\ \mathrm{Re_m} &= \frac{U_\mathrm{m}\ell_\mathrm{m}}{\upsilon_\mathrm{m}} = \mathrm{Re_p} = \frac{U_\mathrm{p}\ell_\mathrm{p}}{\upsilon_\mathrm{p}} \,. \end{aligned} \tag{35.111}$$

The first equation in (35.111) requires that if $\ell_\mathrm{m} < \ell_\mathrm{p}$, then $U_\mathrm{m} < U_\mathrm{p}$, assuming that $g_\mathrm{m} = g_\mathrm{p}$, whereas the second requires that if $\ell_\mathrm{m} < \ell_\mathrm{p}$, then $U_\mathrm{m} > U_\mathrm{p}$, assuming that $\upsilon_\mathrm{m} = \upsilon_\mathrm{p}$. Therefore, unless the gravitational acceleration is considerably increased during the experiments (this is not uncommon considering, for example, some soil-mechanics experiments conducted in a centrifugal apparatus) or ν_m is considerably decreased or some combination of the two, the ratio of Fr to Re can not be held constant simultaneously.

One of the two similarity laws, that is, Froude's law, given by the first equation in (35.111), or Reynolds' law, given by the second, has to be used depending on the particular application in mind. Froude's law (or scale) is generally used in conjunction with the experiments on platform motions and surface waves. Reynolds' law or scale, on the other hand, is used in experiments related to deeply submerged bodies, pipe flow, etc.

Another force mechanism is the surface tension, although it is not a principle one. For example, if we consider the ratio of the inertial force to surface tension force (per unit volume), we obtain

$$\frac{\text{Inertial force}}{\text{Surface tension force}} \propto \frac{\rho u\frac{\partial u}{\partial x}}{\frac{\sigma}{L^2}} \propto \frac{\rho U^2}{\frac{L\sigma}{L^2}} = \frac{\rho L U^2}{\sigma} \,, \tag{35.112}$$

Table 35.5 Some of the frequently used dimensionless numbers

Dimensionless number	Symbol	Definition
Froude number	Fr	$U/\sqrt{gL}$
Reynolds number	Re	UL/υ
Strouhal number	St	fD/U
Keulegan–Carpenter number	KC	UT/D
Euler number	Eu	$p/\rho U^2$
Cauchy number	Cy	$\rho U^2/E$
Ursell number	Ur	HL^2/h^3
Weber number	We	$\rho U^2 L/\sigma$

where σ is the surface tension (lb/ft or N/m). The last equality is called the Weber number, that is

$$\mathrm{We} = \frac{\rho L U^2}{\sigma} \,. \tag{35.113}$$

There are a number of other important numbers used in offshore engineering: the Strouhal number, $\mathrm{St} = fD/U$, where f is the vortex shedding frequency and D is the characteristic length, for example, diameter, and KC number, $\mathrm{KC} = UT/D$, where T is the wave period, are two examples. Some of the dimensionless numbers used are shown in Table 35.5, where U is the velocity, g is the gravitational acceleration, L or D is the characteristic length, f is the cyclic frequency, υ is the kinematic viscosity of water, T is the wave period, H is the wave height, h is the water depth, E is Young's modulus, p is the pressure, and σ is the surface tension.

35.4.2 Scaling of Loads

In planning model tests, one has to decide which scaling law to be used. In most offshore engineering model tests, the Froude scaling law is used as offshore platforms mostly encounter gravity waves in nature. This means that during such experiments, one must make sure to satisfy that $\mathrm{Fr_m} = \mathrm{Fr_p}$. Having also decided what length scale, $S_\mathrm{L} = L_\mathrm{m}/L_\mathrm{p}$, to use, one can scale the other physical quantities, accordingly. For example, if we want to scale the wave forces by using Froude's law, so that $U_\mathrm{m} = U_\mathrm{p} S_\mathrm{L}^{1/2}$, we can first determine the scaling of time and acceleration

$$\begin{aligned} U_\mathrm{m} &= \sqrt{S_\mathrm{L}} U_\mathrm{p} = \frac{L_\mathrm{m}}{t_\mathrm{m}} = \sqrt{S_\mathrm{L}} \frac{L_\mathrm{p}}{t_\mathrm{p}} \Rightarrow t_\mathrm{m} = \sqrt{S_\mathrm{L}} t_\mathrm{p} \,, \\ a_\mathrm{m} &= \frac{U_\mathrm{m}}{t_\mathrm{m}} = \frac{\sqrt{S_\mathrm{L}} U_\mathrm{p}}{\sqrt{S_\mathrm{L}} t_\mathrm{p}} = a_\mathrm{p} \,, \end{aligned} \tag{35.114}$$

where t is the time. That the scales for accelerations are the same in the model and prototype scales is not surprising since the gravitational acceleration in the model and prototype scales is the same, $g_\mathrm{m} = g_\mathrm{p}$.

We also need to scale the masses of the model and the prototype. It is

$$S_\mathrm{m} = \frac{m_\mathrm{m}}{m_\mathrm{p}} = \frac{\rho_\mathrm{m} L_\mathrm{m}^3}{\rho_\mathrm{p} L_\mathrm{p}^3} = S_\rho S_\mathrm{L}^3 \,. \tag{35.115}$$

Therefore, the force scaling can be written as

$$S_\mathrm{F} = \frac{m_\mathrm{m} \dot{U}_\mathrm{m}}{m_\mathrm{p} \dot{U}_\mathrm{p}} = \frac{m_\mathrm{m}}{m_\mathrm{p}} = S_\mathrm{m} = S_\rho S_\mathrm{L}^3 \,, \tag{35.116}$$

since the acceleration scale is 1.0.

This method of obtaining the scaling for forces can be used on any other physical quantity to determine how it is scaled to the model. However, there is another way of obtaining the same scaling result. Let us show this by way of an example. Consider the dimension of force and write it as $[F] = (L, M, T^{-2}) = (1, 1, -2)$, that is, as a vector in the 3-D (L, M, T) space. Writing the functional form of force as $F = f(\rho, L, \mathrm{g})$, and taking the set (ρ, L, g) as a dimensionally independent set of quantities, one can use the Pi theorem [35.75] to obtain the single dimensionless π

$$\begin{aligned} [F] &= (L, M, T^{-2}) = (1, 1, -2) = [\rho]^p \, [L]^q \, [\mathrm{g}]^r \\ &= (-3, 1, 0)^p \, (1, 0, 0)^q \, (1, 0, 2)^r \\ &\text{or} \\ p = 1, q = 3, r = 1 &\Rightarrow \frac{F}{\rho L}^3 \mathrm{g} = \pi \Rightarrow \frac{F_\mathrm{m}}{\rho_\mathrm{m} L_\mathrm{m}^3} \\ &= \frac{F_\mathrm{p}}{\rho_\mathrm{p} L_\mathrm{p}^3} \Rightarrow S_\mathrm{F} = S_\rho S_\mathrm{L}^3 \,. \end{aligned} \tag{35.117}$$

This is the same result given by (35.116).

In Table 35.6, we show the model scales for some of the physical quantities that would be of interest during an offshore engineering experiment (L: length, M: mass, T: time, $S_\mathrm{L} = L_\mathrm{m}/L_\mathrm{p}$ is the length ratio, and $S_\rho = \rho_\mathrm{m}/\rho_\mathrm{p}$ is the specific gravity of salt water). Many others are given in [35.74], but for the special case of $S_\rho = 1.0$.

35.4.3 Elastic Structures

Model tests of elastic structures bring additional complexities to the problem as it is not practical in many cases to correctly scale the stiffness of the structure at the model scale. Such elastic structures could be TLP tendons, oil-production risers, catenary-mooring lines, etc., but the structure itself may be elastic as well, especially very large floating structures (VLFS) [35.76]. To see this, consider a tubular, beam-like object, and write the scalings, from Table 35.6, of the axial and bending

Table 35.6 Some model scaling obtained by using Froude's scaling law

Quantity	Dimension	Scale
Length	L	S_L
Mass	M	$S_\rho S_L^3$
Mass moment of inertia	L^2M	$S_\rho S_L^5$
Moment of inertia of area	L^4	S_L^4
Time	T	$S_L^{1/2}$
Acceleration	LT^{-2}	1
Velocity	LT^{-1}	$S_L^{1/2}$
Linear spring constant	MT^{-2}	$S_\rho S_L^2$
Axial stiffness	LMT^{-2}	$S_\rho S_L^3$
Bending stiffness	L^3MT^{-2}	$S_\rho S_L^5$
Work	L^2MT^{-2}	$S_\rho S_L^4$
Power	L^2MT^{-3}	$S_\rho S_L^{7/2}$
Energy	L^2MT^{-2}	$S_\rho S_L^4$
Force	LMT^{-2}	$S_\rho S_L^3$
Moment	L^2MT^{-2}	$S_\rho S_L^4$
Stress	$L^{-1}MT^{-2}$	$S_\rho S_L$
Pressure	$L^{-1}MT^{-2}$	$S_\rho S_L$
Modulus of elasticity	$L^{-1}MT^{-2}$	$S_\rho S_L$

stiffness, and its diameter as

$$S_{EA} = \frac{(EA)_m}{(EA)_p} = \frac{F_m}{F_p} = S_F = S_m = S_\rho S_L^3 ,$$
$$S_{EI} = \frac{(EI)_m}{(EI)_p} = \frac{F_m L_m^4}{L_m^2}\frac{L_p^2}{F_p L_p^4} = S_F S_L^2 = S_\rho S_L^5 ,$$
$$\frac{D_m}{D_p} = \frac{L_m}{L_p} = S_L . \qquad (35.118)$$

Either the bending or shear stress, τ, is scaled as

$$S_\tau = \frac{F_m}{L_m^2}\frac{L_p^2}{F_p} = \frac{S_F}{S_L^2} = \frac{S_\rho S_L^3}{S_L^2} = S_\rho S_L . \qquad (35.119)$$

And the area moment of inertia is scaled as

$$S_I = \frac{I_m}{I_p} = \frac{L_m^4}{L_p^4} = S_L^4 . \qquad (35.120)$$

Therefore, Young's modulus is scaled as

$$S_E = \frac{E_m}{E_p} = \frac{S_{EI}}{S_I} = \frac{S_\rho S_L^5}{S_L^4} = S_\rho S_L . \qquad (35.121)$$

There are basically two problems one encounters as a result of these scalings. One is that it is very difficult to scale the geometry because D_m is typically 50–100 times smaller than D_p. The other is that the modulus of elasticity of the material used in the experiments is also 50–100 times smaller than what is used in the prototype, for example, steel. Some engineering solutions to these kinds of problems is necessary to conduct the experiments. For example, *Dillingham* [35.77] suggested in modeling the tendons of a TLP that all parameters are correctly scaled for the tendon except the axial stiffness that is modeled by a spring placed at the top or bottom of the tendon to provide the correct stiffness. Even this approximation involves some errors that must be carefully assessed.

The structural rigidity can sometimes be reduced by distorting the structure as discussed, for example, by [35.78]. Another type of a distorted model can be achieved in offshore model tests in rather shallow water where the horizontal length dimensions are much larger than the vertical length dimension. In such cases, two different model scale ratios are used in the experiments [35.74, 79]. Let us again set the horizontal length scale to S_L but set the vertical length scale to $S_V = h_m/h_p$, where h_m and h_p are the water depths in the model and prototype scales, respectively, and S_V, in general, is different from S_L. Next, let us consider the linear shallow-water phase speed, $c_p = (gh)^{1/2}$, and use S_V to write the Froude scaling law to obtain

$$\frac{c_m}{\sqrt{gh_m}} = \frac{c_p}{\sqrt{gh_p}} \Rightarrow c_m = \sqrt{S_V} c_p , \qquad (35.122)$$

and since $c = \lambda/T$, where λ is the wavelength, scaled by S_L, $S_L = \lambda_m/\lambda_p$, we have the following scaling for the wave period

$$\frac{T_m}{T_p} = \frac{\lambda_m}{C_m}\frac{C_p}{\lambda_p} = \frac{S_L}{\sqrt{S_V}} \Rightarrow T_m = \frac{S_L T_P}{\sqrt{S_V}} . \qquad (35.123)$$

If the water is not very shallow, of course, the full dispersion relation based on the linear wave theory can be used in deriving the corresponding scales that will now involve hyperbolic functions. Finally, recall that the accelerations scale as 1.0 if a single length scale is used according to the Froude scaling. In the distorted model used, however, that will not be the case. The accelerations in a distorted model would scale as

$$a_m = \frac{U_m}{T_m} = \frac{\sqrt{S_V} U_p \sqrt{S_V}}{S_L T_p} \Rightarrow \frac{a_m}{a_p} = \frac{S_V}{S_L} . \qquad (35.124)$$

35.5 CFD Tools

With the very rapid advancement in personal and server-based computer hardware and numerical methods, as well as the development of commercial software in recent years, CFD is becoming a viable tool in the computations of wave, current, and wind loads on and the resulting motions of offshore platforms. Here, we use the term CFD to mean the solution of the exact governing equations subject to the instantaneous boundary conditions. The governing equations could be the Reynolds-averaged Navier–Stokes (RANS) equations (steady or unsteady) or Euler's equations in which viscosity is assumed to be negligible, although the definition of CFD computations generally is reserved for viscous flows. We do this since there are many problems in offshore engineering in which the effect of viscosity is negligible.

Even though there is very rapid growth in computer hardware and software, the stumbling blocks in the use of CFD tools are concentrated [35.80] around the user-related problems (some of which are related to training and lack of user-friendly GUI) and theoretical problems (some of which are (1) continuation of computations after wave breaking, (2) radiation/reflection conditions for simulating wave tanks or open ocean conditions, (3) fluid–structure interaction including multiphase flow structural modeling, (4) higher order discretization methods, (5) viscous model selection, which one to use and when, among many other problems). Of course the speed at which the computations can be completed is another major issue even if parallel computing is heavily utilized. It is estimated that by the year 2030 the transistor count will be more than 10^{11} and the computing speed will be more than $1.0E^{+18}$ (Exascale). With the estimated increase in the computing speed, it is expected that the cost of running the same model-scale or full-scale case in the year 2030 would be 250 times less than what it was in the year 2013 for as many as 2500 cores.

With these shortcomings of the field at present, however, there are many commercially available or open-source software that are used to solve problems related to offshore platforms. Some of them are ANSYS AQWA, CD-ADAPCO, Reef3D, FLOW3D, and OpenFOAM. The last open-source software appears to be the most popular one currently, not only because it is free, but also because of its relative ease of use, flexibility, and speed. As examples to the use of OpenFOAM software, see [35.81] for the calculations of wave and current forces (viscous fluid) on a semisubmersible and [35.82] for the calculations of nonlinear (inviscid fluid) wave loads on a coastal bridge deck.

35.6 Extreme Response Estimation

Offshore structure design is based on proportioning a structure so that it resists actions (forces) which may occur during its design life with an appropriate reliability. For a random environment, such as that presented by offshore wind, wave, and current, the extreme loads or responses imposed by the environment are required to assess the fitness of the structure for its intended purpose. A target probability of exceedance in combination with a long-term distribution of the response is used to set these extreme responses.

Annual exceedance probabilities of 10^{-2} or 10^{-4} are used to characterize environmental forces for ultimate and accidental limit states. Scatter diagrams and joint probability density functions are used to describe the variability of forces from multiple sources or with multiple parameters of interest, such as frequency and direction. These diagrams or functions are used to generate combinations of environmental parameters which correspond to exceedance probabilities of interest.

The joint probability of occurrence is used to create combinations of wind, wave, and current conditions causing the extreme loads. For most fixed, tower, gravity, and caisson types of platforms, the design environmental load is predominantly due to waves, with current and wind playing secondary roles. The design conditions comprise the design waves and the currents and winds likely to coexist with the design waves. For compliant structures, response to waves is reduced, so that winds and currents become relatively more important.

For fixed structures, the collinear environment usually controls a design and intensities for various sources of environmental load can be selected from Table 35.7 per [35.83].

For floating installations, environmental conditions that involve large differences in direction need to be considered.

When design forces due to wind need to be combined with forces due to waves and current, the following is appropriate:

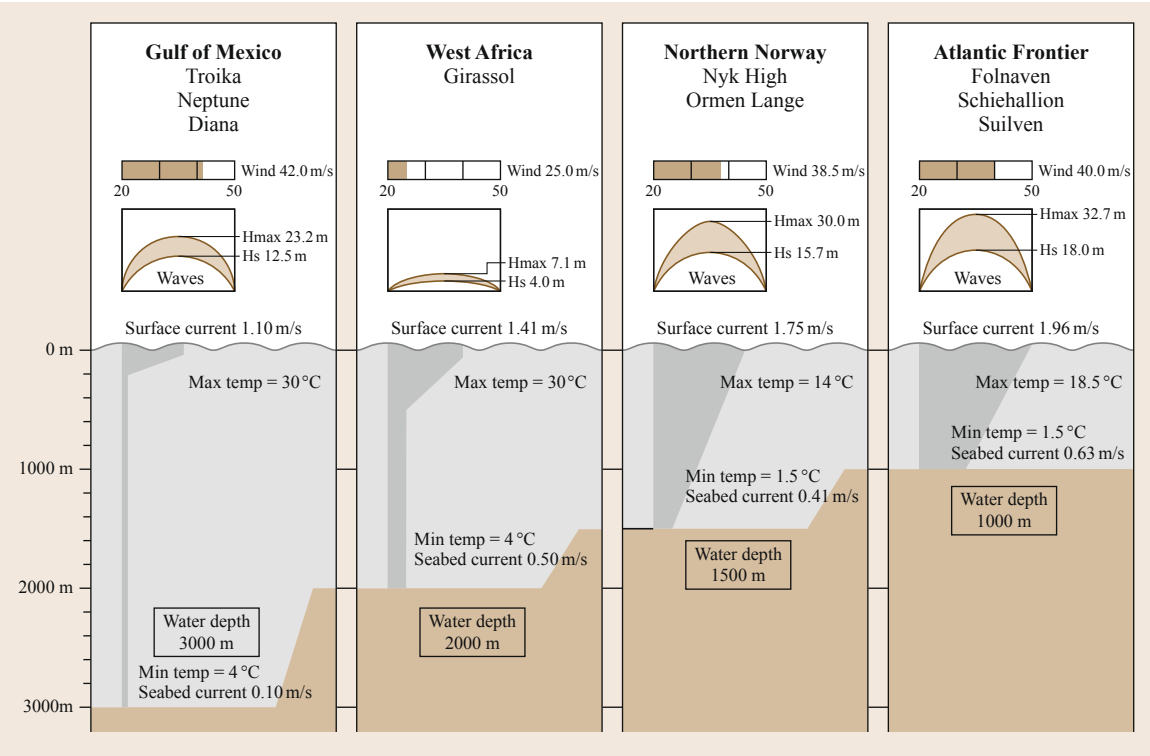

Fig. 35.15 Environmental conditions at a number of deep water sites (after [35.84])

Table 35.7 Combination of environmental forces with expected mean values and annual probability of exceedance

Limit state	Wind	Waves	Current
Ultimate limit state	10^{-2} 10^{-1} 10^{-1} – –	10^{-2} 10^{-1} 10^{-1} – –	10^{-1} 10^{-2} 10^{-1} – –
Accidental limit state	10^{-4} 10^{-2} 10^{-1} – –	10^{-2} 10^{-4} 10^{-1} – –	10^{-1} 10^{-1} 10^{-4} – –

1. For structures with negligible dynamic response, the 1 h sustained wind can be used to determine quasi-static global actions caused by wind in conjunction with ultimate or accidental loads due to waves and currents
2. For structures that are moderately dynamically sensitive, but do not require a full dynamic analysis, the 1 min mean wind can be used to determine quasi-static global loads caused by wind, again for wind in conjunction with ultimate or accidental quasi-static loads due to waves and currents
3. For structures with significant dynamic response to excitation with periods longer than 20 s, a full dynamic response analysis to fluctuating winds should be considered.

Reduced design requirements can be used for the design or relocation of structures that are unmanned or evacuated during the design event or where the loss of or severe damage to the structure would not result in a high consequence of failure. Risk analysis may justify either longer or shorter recurrence intervals for design criteria. Where sufficient information available about the variation under environmental conditions expected to occur from different directions can be considered.

Figure 35.15 illustrates some examples of combined wind, wave, and current environments in four different ocean basins.

References

35.1 G.G. Stokes: On the theory of oscillatory waves, Trans. Camb. Phil. Soc. **8**, 441–455 (1847)
35.2 T. Levi-Civita: Determination rigoureuse des ondes permanentes d'ampleur finie, Math. Ann. **93**, 264–314 (1925)
35.3 L.W. Schwartz: Computer extension and analytic continuation of Stokes' Expansion for gravity waves, J. Fluid Mech. **62**, 553–578 (1974)
35.4 R.L. Wiegel: *Oceanographical Engineering* (Prentice-Hall, New Jersey 1964)
35.5 T. Sarpkaya, M. Isaacson: *Mechanics of Wave Forces on Offshore Structures* (Van Nostrand Reinhold Co., New York 1981)
35.6 L. Skjelbreia, J.A. Hendrickson: Fifth order gravity wave theory, Coast. Eng. Proc. (1960) pp. 184–196
35.7 D.J. Korteweg, G. de Vries: On the change of form of long waves advancing in a rectangular canal, and on a new type of long stationary waves, Phil. Mag. **39**(5), 422–443 (1895)
35.8 E.V. Laitone: The second approximation to cnoidal and solitary waves, J. Fluid Mech. **9**, 430–444 (1960)
35.9 J.E. Chappelear: Shallow water waves, J. Geophys. Res. **67**, 4693–4704 (1962)
35.10 R.C. Ertekin, J.M. Becker: Nonlinear diffraction of waves by a submerged shelf in shallow water, J. Offshore Mech. Arct. Eng. **120**(4), 212–220 (1998)
35.11 J. Boussinesq: Théorie de l'intumescence liquide appelée onde solitaire ou de translation, Comptes Rendus Acad. Sci. Paris **72**, 755–759 (1871)
35.12 J.D. Fenton: A ninth-order solution for the solitary wave, J. Fluid Mech. **53**, 237–246 (1972)
35.13 A.E. Green, N. Laws, P.M. Naghdi: On the theory of water waves, Proc. R. Soc. Lond. A **338**, 43–55 (1974)
35.14 B.B. Zhao, R.C. Ertekin, W.Y. Duan, M. Hayatdavoodi: On the steady solitary-wave solution of the Green–Naghdi equations of different levels, Wave Motion **51**(8), 1382–1395 (2014)
35.15 M.S. Denis, W.J. Pierson: On the motions of ships in confused seas, Trans. Soc. Nav. Archit. Mar. Eng. **61**, 280–357 (1953)
35.16 W.H. Michel: Sea spectra simplified, Mar. Technol. **5**(1), 17–30 (1968)
35.17 O.M. Faltinsen: *Sea Loads on Ships and Offshore Structures*, Ocean Technology Series (Cambridge Univ. Press, Cambridge 1990)
35.18 J.N. Newman: *Marine Hydrodynamics* (MIT Press, Cambridge 1978)
35.19 S.K. Chakrabarti: *Hydrodynamics of Offshore Structures* (Comput. Mechanics, Southampton 1987)
35.20 L.L. Huang, H.R. Riggs: The hydrostatic stiffness of flexible floating structures for linear hydroelasticity, Mar. Struct. **13**, 91–106 (2000)
35.21 R.C. Ertekin, H.R. Riggs, X.L. Che, S.X. Du: Efficient methods for hydroelastic analysis of very large floating structures, J. Ship Res. **37**(1), 58–76 (1993)
35.22 J.V. Wehausen: The motion of floating bodies, Ann. Rev. Fluid Mech. **3**, 237–268 (1971)
35.23 H. Goldstein: *Classical Mechanics*, 2nd edn. (Addison-Wesley, Reading 1980)
35.24 R.W. Yeung: *A Singularity-Distribution Method for Free-Surface Flow Problems with an Oscillating Body*, Rep. No. 73-6 (University of California, Berkeley 1973)
35.25 O.M. Faltinsen, F.C. Michelsen: Motions of large structures in waves at zero Froude number, Int. Symp. Dyn. Mar. Veh. Struct. Waves (1974) pp. 91–106
35.26 C.J. Garrison: Hydrodynamic loading of large offshore structures: Three-dimensional source distribution methods. In: *Numerical Methods in Offshore Engineering*, ed. by O.C. Zienkiewicz, R.W. Lewis, K.G. Stagg (Wiley, New York 1978)
35.27 J.V. Wehausen, E.V. Laitone: Surface waves. In: *Handbuch der Physik*, Vol. 9, ed. by S. Flugge (Springer, Berlin, Heidelberg 1960)
35.28 J.N. Newman: Algorithms for the free-surface Green function, J. Eng. Math **19**, 57–67 (1985)
35.29 C.A. Brebbia: *The Boundary Element Method for Engineers* (Wiley, New York 1978)
35.30 A.E. Cummins: The impulse response function and ship motions, Schiffstechnik **9**(47), 101–109 (1962)
35.31 T.F. Ogilvie: Recent progress toward the understanding and prediction of ship motions, Proc. 5th Symp. Nav. Hydrodyn. (1964) pp. 3–79
35.32 J.O. de Kat, J.R. Paulling: The simulation of ship motions and capsizing in severe seas, Soc. Nav. Archit. Mar. Eng. **97**, 139–168 (1989)
35.33 R.F. Beck: Time-domain computations for floating bodies, Appl. Ocean Res. **16**, 267–282 (1994)
35.34 J. Nolte, R.C. Ertekin: Wave power calculations for a wave energy conversion device connected to a drogue, J. Renew. Sustain Energy (AIP) **6**(1), 013117-1–013117-21 (2014)
35.35 H. Maruo: Thel drift of a body floating on waves, J. Ship Res. **4**(1), 1–10 (1960)
35.36 J.N. Newman: The drift force and moment on ships in waves, J. Ship Res. **6**(1), 10–17 (1967)
35.37 J.A. Pinkster: Mean and low frequency wave drifting forces on floating structures, Ocean Eng. **6**, 593–615 (1979)
35.38 C.J. Garrison: *Hydrodynamic interaction of waves with a large displacement floating body*, Rep. No. NPS-69GM77091 (Naval Postgraduate School, Monterey 1977)
35.39 M. Takaki, Y. Tango: Wave drift forces on very huge floating structures, Int. J. Ofshore Polar Eng. **5**(3), 204–211 (1995)
35.40 X.Q. Liu, R.C. Ertekin, H.R. Riggs, D. Xia: Mean wave-drift loads on connected semisubmersible modules, Proc. 17th Int. Conf. Offshore Mech. Arct. Eng. (OMAE) (1998)
35.41 F.H. Hsu, K.A. Blenkarn: Analysis of peak mooring forces caused by slow vessel drift oscillations in random seas, Offshore Technol. Conf. (1970) pp. 135–146
35.42 J.N. Newman: Second-order slowly varying forces on vessels in irregular waves, Int. Symp. Dyn. Mar. Veh. Struct. Waves (1974) pp. 182–186

35.43 J.R. Morison, M.P. O'Brien, J.W. Johnson, S.A. Schaaf: The force exerted by surface piles, Petroleum Trans. **189**, 149–154 (1950)

35.44 R.C. MacCamy, R.A. Fuchs: *Wave Forces on Piles: A Diffraction Theory*, Tech. Memo. No. 69 Beach Erosion Board (Army Corps of Engineers, Washington 1954)

35.45 G.H. Keulegan, L.H. Carpenter: Forces on cylinders and plates in an oscillating fluid, J. Res. Nat. Bureau Stand. **60**(5), 423–440 (1958)

35.46 M. de S.Q. Isaacson: Wave Induced Forces in the Diffraction Regime. In: *Mechanics of Wave-Induced Forces on Cylinders*, ed. by T.L. Shaw (Pitman, London 1979) pp. 68–89

35.47 J.R. Paulling: Frequency-domain analysis of otec CW pipe and platform dynamics, Offshore Technol. Conf. (1979) pp. 1641–1651

35.48 J.R. Paulling: An equivalent linear representation of the forces exerted on the OTEC CW pipe by combined effects of waves and current, Ocean Eng. OTEC (1979) pp. 21–28

35.49 L.P. Krolikowski, T.A. Gay: An improved linearization technique of frequency domain riser analysis, Offshore Technol. Conf. (1980) pp. 341–353

35.50 T. Sarpkaya: *Wave Forces on Offshore Structures*, 1st edn. (Cambridge Univ. Press, Cambridge 2010)

35.51 T. Sarpkaya: *In-Line and Transverse Forces on Smooth and Sand-Roughned Cylinders in Oscillatory Flow at High Reynolds Numbers, Rep. No. NPS-69SL76062* (Naval Post Graduate School, Monterey 1976)

35.52 DNV: *Recommended Practice DNV-RP-025. Environmental Conditions and Environmental Loads* (Det Norske Veritas, Høvik 2010)

35.53 S.K. Chakrabarti: Steady drift force on vertical cylinder–viscous vs. potential, Appl. Ocean Res. **6**, 73–82 (1984)

35.54 G.E. Burns: Calculating viscous drift of a tension leg platform, Proc. 2nd Int. Offshore Mech. and Arct. Eng. Conf., ASME, Houston (1983) pp. 22–30

35.55 D.L.R. Botelho, T.D. Finnigan, C. Petrauskas, S.M. Lui: Model test evaluation of a frequency-domain procedure for extreme surge response prediction of tension leg platforms, Proc. 16th Annual Offshore Technol. Conf., Houston, Texas OTC 4658 (1984) pp. 105–112

35.56 R.C. Ertekin, A.S. Chitrapu: Wave- and current-induced viscous drift forces on floating platforms, Proc. 6th Int. Symp. Offshore Eng. (1987) pp. 625–629

35.57 A.S. Chitrapu, R.C. Ertekin, J.R. Paulling: Viscous drift forces in regular and irregular waves, Ocean Eng. **20**(1), 33–55 (1993)

35.58 Y. Li, A. Kareem: A description of hydrodynamic forces on tension leg platforms using a multivariate Hermite expansion, Proc. 9th Int. Offshore Mech. Arct. Eng. Conf. (1990) pp. 133–142

35.59 P.D. Spanos, M.G. Donley: Stochastic response of a tension leg platform to viscous drift forces, Proc. 9th Int. Offshore Mech. Arct. Eng. Conf. (1990) pp. 107–114

35.60 NDBC: Does NDBC measure ocean current velocities?, http://www.ndbc.noaa.gov/adcp.shtml (2013)

35.61 B. Bischof, E. Rowe, A.J. Mariano, E.H. Ryan: The Brazil current, http://oceancurrents.rsmas.miami.edu/atlantic/brazil.html (2004)

35.62 G.Z. Forristall, C.K. Cooper: Design current profiles using Empirical Orthogonal Functions (EOF) and Inverse FORM methods, Offshore Technol. Conf. (1997)

35.63 J.T. Kirby, T.M. Chen: Surface waves on vertically sheared flows, approximate dispersion relations, J. Geophys. Res. **94**(C1), 1013–1027 (1989)

35.64 R.A. Dalrymple, J.C. Heideman: Non-linear water waves on a vertically-sheared current, E&P Forum Workshop (1989)

35.65 J.W. Eastwood, C.J.H. Watson: Implications of wave-current interactions for offshore design, E&P Forum Workshop (1989)

35.66 J.D. Wheeler: Method for calculating force produced by irregular waves, J. Petroleum Tech. **22**, 473–486 (1970)

35.67 A.R.Pf. Planning: *Designing and Constructing Fixed Offshore Platforms: Working Stress Design*, 21st edn. (American Petroleum Institute, Washington 2000)

35.68 H. Schlichting: *Boundary Layer Theory*, 2nd edn. (McGraw-Hill, New York 1968)

35.69 R.D. Blevins: *Flow-Induced Vibration*, 2nd edn. (Van Nostrand Reinhold, New York 1990)

35.70 DNV: *Recommended Practice DNV-RP-F105. Free Spanning Pipelines* (Det Norske Veritas, Nøvik 2006)

35.71 DNV: *Recommended Practice DNV-RP-F204. Riser Fatigue* (Det Norske Veritas, Nøvik 2005)

35.72 NRCS: Wind Rose Data, http://www.wcc.nrcs.usda.gov/climate/windrose.html (2002)

35.73 O.J. Andersen, J. Løvseth: The Frøya database and maritime boundary layer wind description, Mar. Struct. **19**(2/3), 173–192 (2006)

35.74 S.K. Chakrabarti: *Offshore Structure Modeling* (World Scientific, Singapore 1994)

35.75 E. Buckingham: On physically similar systems; illustrations of the use of dimensional equations, Phys. Rev. **4**(4), 345–376 (1914)

35.76 R.C. Ertekin, J.W. Kim (Eds.): *The Proceedings of 3rd International Workshop on Very Large Floating Structures (VLFS '99)* (SOEST, Honolulu 1999)

35.77 J.T. Dillingham: Recent experience in model-scale simulation of tension-leg platforms, Mar. Technol. **21**(2), 186–200 (1984)

35.78 M.P. Tulin: Hydroelastic scaling, Proc. 3rd Int. Workshop Very Large Float. Struct. (VLFS) (1999) pp. 483–487

35.79 S.A. Hughes: *Physical Models and Laboratory Techniques in Coastal Engineering* (World Scientific, Singapore 1993)

35.80 W.Y. Duan: Report of the 1st workshop on numerical wave tank, Int. Theory Advis. Panel Numer. Tank (College of Shipbuilding Engineering, Harbin Engineering University, Harbin, China 2014)

35.81 M.A. Benitz, D.P. Schmidt, M.A. Lackner, G.M. Stewart, J. Jonkman, A. Robertson: Comparison of hydrodynamic load predictions between engineering models and computational fluid dynamics for the

Oc4-DeepCWind semi-submersible, Proc. 33rd Int. Offshore Mech. Arct. Eng. Conf. (OMAE) (2014)
35.82 B. Seiffert, M. Hayatdavoodi, R.C. Ertekin: Experiments and computations of solitary-wave forces on a coastal-bridge deck. Part I: Flat plate, Coast. Eng. **88**, 194–209 (2014)
35.83 S. Norway: *NORSOK Standard N-003: Actions and action effects* (Standards Norway, Lysaker 2007)
35.84 A. Moros, P. Fairhurst: Production riser design: Integrated approach to flow, mechanical issues, Offshore Mag. **59**(4), 82 (1999)